This Page Is Inserted by IFW Operations
and is not a part of the Official Record

BEST AVAILABLE IMAGES

Defective images within this document are accurate representations of the original documents submitted by the applicant.

Defects in the images may include (but are not limited to):

- BLACK BORDERS
- TEXT CUT OFF AT TOP, BOTTOM OR SIDES
- FADED TEXT
- ILLEGIBLE TEXT
- SKEWED/SLANTED IMAGES
- COLORED PHOTOS
- BLACK OR VERY BLACK AND WHITE DARK PHOTOS
- GRAY SCALE DOCUMENTS

IMAGES ARE BEST AVAILABLE COPY.

As rescanning documents *will not* correct images, please do not report the images to the Image Problem Mailbox.

THIS PAGE BLANK (USPTO)

DK 00/140
4

REC'D 18 APR 2000
WIPO PCT

Kongeriget Danmark

Patent application No.: PA 1999 00749

Date of filing: 27 May 1999

Applicant: Leif Østergaard Harees
Jacob Knudsens Vej 5
DK-8230 Aabyhøj

This is to certify the correctness of the following information:

The attached photocopy is a true copy of the following document:

- The specification, claims and drawings as filed with the application on the filing date indicated above.

PRIORITY DOCUMENT
SUBMITTED OR TRANSMITTED IN COMPLIANCE WITH RULE 17.1(a) OR (b)

Patent- og Varemærkestyrelsen • Kongeriget Danmark •

Patent- og
Varemærkestyrelsen
Erhvervsministeriet

Taastrup 06 April 2000

Karin Schlichting
Head Clerk

PLOUGMANN, VINGTOFT & PARTNERS

COPENHAGEN OFFICE:
SANKT ANNÆ PLADS 11
POST OFFICE BOX 3007
DK - 1021 COPENHAGEN K
A/S REG. NO. 223795
TELEPHONE +45 33 63 93 00
TELEFAX +45 33 63 96 00
e-mail pv@pv.dk

Modtaget PD
27 MAJ 1999

Artist Bjørn Bjerrisgård

AARHUS OFFICE:
RÅDHUSPLADSEN 1
POST OFFICE BOX 49
DK - 8100 AARHUS C
TELEPHONE +45 87 32 18 00
TELEFAX +45 33 63 96 00
e-mail pv@pv.dk

27. maj 1999

Ny dansk patentansøgning
Leif Østergaard Harees
Method for determining haemodynamic indices by use of tomographic data
Vor ref: 22872 DK 1

Plougmann, Vingtoft & Partners

Ole Plougmann
Knud Erik Vingtoft
Anne Pors
Henrik Rastrup Andersen
Jeff Salka
Anne Schouboe
Henry Sagaard
Marianne Johansen
Michael Gaarmann
Gert Høy Jakobsen
Annemette Biermann
Anne-Marie Lademann
Susie P. Arnesen
Jan Simonsen
Jesper Thomsen

Inge Uhorius
Nanna Wigil
Jakob Pade Frederiksen
Per Jørgen Nygreen
Kim Wagner
Camilla Rendal Nielsen
Jens Jørgen Schmidt
Steen Madsen
Martin Hancock
Anja Grünbaum
Heidi Petersen
Flemming Vestor
Chrisa Theil
Nikolas Krogh
Henrik Bagger Olsen
Peter Laudrup
Peter Hom Møller
Tom Friis-Mikkelsen
Ole Christian Madsen
Pia Nørregaard J. Ruggles

Stephen H. Addinson, Boston

Manager of Finance
Jan Hammer

Patents Trademarks Designs Copyright Licensing Documentation
European Patent Attorneys European Trademark Attorneys
Copenhagen Aarhus Munich Reykjavik Boston Alicante

METHOD FOR DETERMINING HAEMODYNAMIC INDICES BY USE OF TOMOGRAPHIC DATA

The present invention relates to a method for determining haemodynamic indices of an organ or a part of tissue of a mammal, such as a human being, from a time series of tomographic data, especially data obtained by means of Magnetic Resonance Imaging (MRI). The method produces maps of distribution of blood transit time as well as other indices being significant of the dynamics of the capillary tissue flow from tomographic images acquired during rapid bolus injection of a contrast agent or tracer that stays mainly intravascular in the organ. The haemodynamic indices may by use of the present method be obtained with a spatial resolution equal to the spatial resolution of the tomographic data.

The method comprises the steps of conversion of tomographic images into data representing concentrations of contrast agent as a function of time, and the method determines the distribution of flow and mean transit time, either in absolute values or relative to the mean value, whereby the methods facilitates the (i) comparison of relative flow distributions to that of other tissue (in particular cerebral tissue), such as normal tissue, or (ii) quantification of absolute flow distributions in terms of the associated extraction of a substance with known capillary permeability.

The use of the methods for examination and monitoring of cerebral conditions of humans are of particular interest, but the method may also be applied to other organs, such as the heart, the liver, kidneys etc., or to other part of tissue or part of organs.

BACKGROUND

Microscopic heterogeneity of flow is believed to be a main determinant of how efficient the delivery of nutrients and pharmaceuticals to tissue takes place. Especially in diseases where delivery of nutrients such as e.g. oxygen is compromised, determination of flow heterogeneity is therefore crucial to assess the severity of the disease. Such diseases include acute cerebral ischemia, a frequent cause of death and the major cause of adult neurological disability in the Western world.

So far, the measurement of flow heterogeneity has been limited to the study to superficial vessels in the cortex of anaesthetised animals by high-speed intravital microscopy. There are no pre-existing tools that allow determination flow heterogeneity in deeper structures, or on humans as part of non-invasive, routine diagnostic procedures.

The study of the delivery of nutrients to the tissue is currently done by Positron Emission Tomography (PET). Due to the costs and lack of general availability of this technique, these studies can, however, not be performed in general patient management.

A major limiting factor in the development of new drugs in many diseases is the cost of preclinical and clinical trials to determine beneficial effects of new agents. In acute stroke, this is typically done by comparing long-term neurological scores of thousands of treated and untreated patients. The costs of this work, as well as the total number of patients available, therefore limits the rate at which novel drugs become available for common use. There exists therefore an urgent need for techniques that in individual patients predict the progression of a disease or condition and may be used for monitoring of said progression, so that the progression for the individual patient can be assessed whereby e.g. the efficacy of a drug or a substance can be evaluated in details from a much more limited number of patients. Such techniques are not currently available.

With the spatial resolution of some tomographic imaging techniques, the dimensions of vessels are too small to accurately determine arterial tracer concentration levels non-invasively. Instead, image elements containing partly tissue, partly blood vessels must be used in order to characterise the mere shape of the arterial input curve to the tissue. In such cases, absolute values of flow and volume cannot be found, and therefore a normalisation routine allowing (i) comparison of serial measurements in a single subject, (ii) comparison among subjects and (iii) absolute quantification the case of susceptibility MRI of the brain is necessary as described below.

The present invention describes and validates a new, non-invasive method that allows assessment of flow heterogeneity on generally available tomographic equipment

(Magnetic Resonance (MR), Computed Tomography (CT), PET). Furthermore, the technique allows indirect assessment of metabolic parameters.

Finally, the technique has high predictive power in terms of disease progression in cerebral diseases such as ischemia, thereby providing the means for rapid assessment of the efficacy of novel therapies.

DESCRIPTION OF THE INVENTION

It is an object of the present invention to provide a method for determining haemodynamic indices of an organ or part of tissue of a mammal, such as a human being from tomographic data.

By haemodynamic indices is understood such indices as distribution of transit times and parameter characterising said distribution, quantitative haemodynamic parameters obtained from said distribution such as parameters characterising the deviation of said distribution from a reference distribution, as well as other indices being significant of the dynamics of the capillary tissue flow.

It is a further object of the present invention to facilitate the comparison of relative flow distributions to a predetermined distribution found for a normal organ (e.g. the brain) or for an organ having a recognised disease or condition, such as having a tumour of an identified tumour type.

It is a still further object of the present invention to provide quantification of absolute flow distributions in terms of the associated extraction of a substance with known capillary permeability.

It is a yet still further object of the present invention to provide the above methods so that they are applicable to human cerebral tissue.

Thus, the present invention relates to a method for determining haemodynamic indices of an organ or part of tissue of a mammal including

a) determining a time series of tomographic data pertaining to the organ or part of tissue during and after a bolus injection of a tracer dose to said mammal, the tracer being substantially intravascular in said tissue,

b) determining a time series of concentration data being indicative of the concentration of the tracer in arteries of the organ or tissue from the time series of tomographic data,

c) determining a residue function of the organ or of the part of tissue by deconvolution of the time series of tomographic data with the time series of concentration data, and

d) determining a distribution of transit times from the slope of the residue function.

The residue function may also be understood as a normalised impulse response function characterising the fraction of the tracer present in the vascular tissue at time *t* after a perfect, infinitely sharp input of a tracer in the feeding vessel. For the deconvolution a number of known methods may be applied, such as a Fourier transform, Box transform, but preferably the Singular Value Decomposition is used.

The distribution of transit times obtained from this method may be used to determine a probability density function (PDF) of a normalised haemodynamic index, where the index is normalised by the value of the integral of this index.

One of the haemodynamic indices obtained from the PDF may be a quantitative haemodynamic parameter, such as a parameter obtained from comparison of the determined PDF and a previously determined reference PDF, e.g. obtained by use of the Kolmogorov Smirnov test. The comparison between the determined PDF and a reference may also include identification of plateau's of the curve of the PDF, distribution of area under the curve, area under the curve at one or the other side of a cut-off value, etc.

The predetermined reference PDF used for comparison may have been found for a normal organ (e.g. the brain) or tissue or for an organ having a recognised disease or condition, such as having a tumour of an identified tumour type.

Furthermore, the present invention relates to a method in which the quantitative parameter may be obtained by performing the steps of

determining the impulse response function of the organ or of the part of tissue by deconvolution of the time series of tomographic data with the time series of concentration data,

determining the relative tissue flow from the impulse response function of the organ or of the part of tissue,

normalising said time series of concentration data with the integral of said time series of concentration data with respect to time,

determining the normalised relative tissue flow, respectively the normalised blood volume, of the organ or part of tissue by use of the relative tissue flow and the time series of normalised concentration data, and

converting said normalised relative tissue flow, respectively normalised blood volume, to an absolute value for the tissue flow, respectively the blood volume, by means of a previously determined conversion factor,

the quantitative haemodynamic parameter being of metabolic significance and determined from the PDF and the absolute tissue flow, respectively the absolute blood volume.

The normalised relative tissue flow obtained from this method may be used to compare tissue flow determined from successive tomographic scanning of the same mammal in order to monitor the development of a condition of an organ or part of tissue and/or to compare tissue flow of different individuals. The comparison may be performed because the data have been normalised which means that they are readily comparable.

The blood volume is obtained by dividing the blood flow by the mean transit time (MTT) or as the area under the tissue concentration curve (or the impulse response function) of the first pass of the bolus tracer passage.

It is understood that the tomographic data may be obtained from a variety of methods, of which MRI and Computed Tomography (CT) are preferred. However, for some applications it may be preferred to use other methods, such as Positron Emission Tomography (PET) or Single Photon Emission Computed Tomography (SPECT).

The above method may further comprise a step, wherein the normalised relative tissue flow, respectively the blood volume, is also normalised with the ratio between body weight of the individual mammal and the injected tracer dose. By adding this step, the determined relative tissue flow is furthermore made comparable to determined relative tissue flow from tomography time series of the same individual mammal in which the amount of the injected tracer dose have been changed. The relative tissue flow determined for one individual mammal may furthermore be compared to relative tissue flows determined for other individuals.

The conversion factor may be a factor that is generally applicable for the present method to members of a mammalian specie.

In particular, the conversion factor may be a factor that is generally applicable for the present method to an organ or tissue of the mammalian specie.

As a special case, a parameter (E) significant for the local extraction of a substance may be determined by a method further comprising the following steps:

calculating the relative flow heterogeneity (w(f)) as a function of the relative flow (f) from the distribution of transit times,

estimating a value (P) for the local capillary permeability,

estimating a value (S) for the local capillary surface area,

calculating said parameter (E) as the integral value of the relative flow heterogeneity (w(f)) multiplied by one minus the natural exponential function of the negative ratio between

i) the product of the local capillary permeability (P) and the local capillary surface area (S), and

ii) the product of the relative flow (f) and the absolute tissue flow (F_t)

with respect to the relative flow (f).

The substance in question may, e.g., be oxygen, glucose or another important cellular metabolic substance or it may, e.g., be a drug or another substance having a therapeutic effect.

Estimated values of the local capillary permeability (P) and the local capillary surface area (S) are well-known and may be found from standard works within the subject area.

The tomography data for the method according to the invention are preferably obtained by means of magnetic resonance imaging, and the method is furthermore preferably applied to cerebral tissue. For cerebral tissue, it has been found to be advantageous to obtain the tomographic data by means of susceptibility contrast magnetic resonance imaging.

The predetermined conversion factor may be a constant factor applicable for the present method for any organ or any part of tissue of the mammalian specie. Preferably, the predetermined conversion factor is a constant factor applicable for all of cerebral tissue of the mammalian specie, which is strongly indicated from empirical evidence.

The tomographic data discussed above and used in the present method will normally comprise information pertaining to subregions of sections of the organ or part of tissue and the haemodynamic indices are determined for at least a substantial part of said subregions. The data of the subregions may be represented graphically as pixel values (as a gray-scale image or colour image of the section), and the quantitative haemodynamic parameter determined from the tomograpic data may also be represented as images subdivided into a plurality of pixels each representing a quantitative haemodynamic parameter pertaining to one of said subregions.

The present invention furthermore relates to a system for processing of time series of tomographic data pertaining to an organ or a part of tissue according to one or more of the above described methods according to the invention, said system residing on a computer having means for producing an output representative of at least some of the determined haemodynamic indices.

The present invention further relates to a method for evaluating the efficacy of a drug or a substance on an organ or on a part of tissue of a mammal by means of haemodynamic indices of said organ or of said part of tissue obtained by one or more of the methods according to the invention as described above. For this use, a system residing on a computer as described in the previous paragraph may advantageously be applied.

The present invention further relates to a method for obtaining information of the likelihood of recovery of an organ or part of tissue in a living mammal upon or during a period of insufficient vascular supply of said organ or of said part of tissue in the mammal comprising determining haemodynamic indices by one or more of the methods according to the invention as described above.

The present invention further relates to a method for obtaining information relevant for discrimination between relevant therapy of an organ or part of tissue in a living mammal upon or a period of insufficient vascular supply of said organ or of said part of tissue in the mammal comprising determining haemodynamic indices by one or more of the methods according to the invention as described above.

Furthermore, the present invention relates to the use of information obtained by use of one or more of the methods according to the invention as described above for preparing a reference table for use in discrimination of a treatment schedule for an individual mammal or group of mammals for which information have been obtained in a manner similar to said information.

The equipment for performing the tomographic data for use in the method according to the present invention is general standard equipment available to such an extent that the method can be applied in routine patient management. In addition, the

determination may be performed easily and rapidly for healthy as well severely ill patients such as patients in coma. The method may be used for diagnosis and evaluation of possible further progress of disease whereby a suitable treatment schedule may be applied.

The present method is useful in connection with detection of heterogeneity of transit times, velocities or flows by means of external detection of tracers in general, whether in biological or technical systems. The technique is applicable to the diagnosis and study of a number of diseases, as well as in the development and subsequent monitoring of therapies in these diseases. Examples include:

(i) Diagnosis and treatment of diseases where, due to altered blood supply, tissue flow dynamics and thereby flow heterogeneity of an organ is altered, e.g. myocardial infarction, acute stroke, migraine, carotid stenosis, dementia.

In particular the method may be used in connection with prediction/assessment of subsequent tissue damage based on heterogeneity measurements in the acute phase of myocardial or cerebral infarction, evaluation of drug efficacy in these diseases based on predictions as to the subsequent progression of the disease by heterogeneity measurements, and planning treatment based on prior knowledge of flow or transit time heterogeneity and the associated risk of amelioration of disease.

(ii) Diagnosis, study and treatment of diseases that alter or interfere with vascular architecture in any organ or pathological tissue, such that normal flow or transit time heterogeneity is disturbed, e.g.: (a) Angiogenesis (the formation of new vessels) by tumors, where the random formation of irregular vessels causes increased heterogeneity of flows due to the passage through irregular vascular paths. (b) Vasculopathies, i.e. diseases where normal vascular wall architecture is disrupted, altering the passage and thereby flow heterogeneity of blood or tracer molecules, such as collagen vascular diseases (Systemic lupus erythematosus, rheumatoid arthritis, other connective tissue disorders), vasculitis (giant cell arteriritis, polymylagia rheumatica), micro- and macroangiopathies in diabetes, angiopathy due to hypertension. (c) Changes in vascular architecture due to chronic or degenerative processes of organs (liver, kidneys, heart, brain) in general.

In particular the method may be used in connection with assessment of disease stage (e.g. tumor grade) based on heterogeneity measurements, evaluation of drug efficacy in these diseases based on quantification of heterogeneity measurements (e.g. anti-angiogenic treatment), and planning treatment based on prior knowledge of flow or transit time heterogeneity and the associated risk of amelioration of disease.

In connection with organ transplantations it is generally of great value to know the vascular supply and the capacity of the vascular system of the organ.

(iii) The study of extraction of solutes in normal or diseased tissue as part of diagnosis or treatment. The technique can – given the capillary permeability of a particular solute - be applied to a given organ, providing the regional extraction of the solute. Examples include the study of oxygen, glucose or pharmaceutical uptake in the normal or diseased brain, e.g. acute or chronic ischemia, dementia, Parkinsons disease.

Accordingly, the invention relates to a method for identifying a condition relating to haemodynamic changes in an organ or tissue of a mammal, diagnosis of disease, treatment or prevention of disease, monitoring of disease, and for screening of a pharmaceutically active drug. The method involves use of the determination the tissue flow as described herein.

DETAILED DESCRIPTION OF PREFERRED METHODS ACCORDING TO THE INVENTION

The present method produces maps of normalised relative or absolute tissue blood flow, blood volume and absolute blood mean transit time from dynamic, tomographic images acquired during rapid bolus injection of a contrast agent or tracer that stays mainly intravascular in the organ.

By 'blood volume' is understood tracer or contrast agent distribution volume per tissue volume. If the distribution volume is less than that of total blood (e.g. only plasma), it is understood that conversion to absolute blood volume can be achieved by knowledge of regional distribution volume characteristics, e.g. haematocrit, or other

normalisation by an independent techniques (e.g. positron emission tomography) as presented in this description. Likewise, 'blood flow' refers to flow of tracer or contrast agent distribution volume per tissue volume per unit time, with the aforementioned method of conversion to blood flow. Finally, 'transit time' refers to the time taken for tracer or contrast agent to traverse the image element, the arrival at which is defined from the arterial input measurement.

Furthermore, the method determines the *distribution* of flow and mean transit time, either in absolute values or relative to the mean value. The methods further allows the (i) comparison of relative flow distributions to that of normal tissue (here brain) or (ii) quantification of absolute flow distributions in terms of the associated extraction of a substance with known capillary permeability.

With the resolution of some tomographic imaging techniques, the dimensions of vessels are too small to accurately determine arterial tracer concentration levels non-invasively. Instead, image elements containing partly tissue, partly blood vessels, must be used in order to characterise the mere shape of the arterial input curve to the tissue. In such cases, absolute values of flow and volume cannot be found, and therefore a normalisation routine allowing (a) comparison of serial measurements in a single subject, (b) comparison among subjects and (c) absolute quantification the case of susceptibility MRI of the brain is described below.

OVERVIEW

The techniques consist of the following steps:

A. Conversion of tomographic images into images representing concentrations of contrast agent as a function of time.

B. Identification of relative or absolute (i.e. in units identical to those of the tomographic images) arterial tracer concentrations from the image data.

C. In the case of *relative* arterial tracer concentrations, normalisation of the arterial input area to the injected dose of contrast agent per kg body weight.

D. Optional correction of tissue tracer curves for delays.

E. Determination of

(i) absolute or relative tissue blood flow

(ii) tissue impulse response function

by deconvolution of tissue concentration time curves by the arterial tracer concentration in each image element.

F. Determination of tissue blood volume by determining the area under the tissue first-pass concentration curve.

G. Determination of tissue mean transit time.

H. In the case of MR susceptibility contrast imaging using Gd-chelates in brain tissue, conversion to absolute blood flow and blood volume by a pre-determined constant.

I. Determination of the distribution of flow or transit times in each image element from the residue function (normalised impulse response function) determined in E.

J. Comparison of distributions of relative flows to a predetermined distribution found for a normal organ; here brain.

K. Quantification of the distribution of flows in terms of the extraction fraction of a given solute with specified capillary permeability, in cases where imaging is performed with MR imaging with microvascular weighting, or microvascular volume can otherwise be inferred from total blood volumes.

1. Conversion of tomographic data into tracer concentration images

The method and associated software handles various modalities, depending on whether tracer injection changes signal intensity from baseline in a linear or logarithmic fashion upon tracer arrival. With a specified option, acquired tomographic images during tracer bolus injection are converted into concentrations as a function of time, with measurement time points spaced equally in time.

1.1. In the case of MR images, weighted towards the transverse relaxation times (T_2 or T_2^*), (typically acquired in brain), the tissue concentration as a function of time, $C_t(t)$, is typically obtained by the formula

$$C_t(t) = -k \cdot \log\left(\frac{S(t)}{S(t_o)}\right) / TE \qquad \text{Eq. 1}$$

where $S(t_0)$ is the signal intensity before contrast injection (formed as the average of signal intensities up to tracer arrival), $S(t)$ is the signal intensity at time t, and TE is the echo time used in the sequence. Here, k is a constant characteristic of the tissue and contrast agent.

1.2. In the case of MR images weighted towards the longitudinal relaxation time (T_1) images (typically acquired for intravascular tracers in the heart), concentrations are assessed directly by the change in longitudinal relaxation rate, ΔR_1

$$C_t(t) = \Re \cdot \Delta R_1 \qquad \text{Eq. 2}$$

where $\Re$ is the relaxivity of the applied contrast agent.

1.3. In the case of Computed Tomography (CT) images, concentrations are assessed by the change in image intensity, measured in Hounsfield units, ΔH

$$C_t(t) = \kappa \cdot \Delta H \qquad \text{Eq. 3}$$

where κ is the characteristic X-ray absorption of the contrast agent.

2. Identification of Arterial Vessels

For identification of arterial vessels in the image, the algorithm provides the choice of first producing an image that guides this process (2.a.), or proceeding directly to calculation of tissue flow (2.b.)

2.a. If so specified by an option, the concentration time curve of each image element is fitted to a gamma variate function by nonlinear least-squared regression (by means of a fletcher-algorithm) over the time interval until visible tracer re-circulation occurs (the re-circulation is specified by the user, determining

(a) Tracer arrival time.

(b) Area under first pass (this quantity is proportional to the local blood volume).

These two quantities are stored as floating point binary image file, allowing visualisation as an image where each image pixel corresponds to quantities (a) and (b), respectively. An artery is then visually identified in these images by

(a) Anatomical location.

(b) Early tracer arrival relative to the arrival in tissue.

(c) Large area under first pass (corresponding to a large blood volume and thereby a large portion of the vascular volume being contained in a voxel).

2.b. By observing images of tracer concentration as a function of time in a tool that allows visualisation of the time-course of single pixels, arterial levels can be identified.

Upon identification of the arterial input function, the corresponding signal intensity time curve is fed to the program below in the form of an ASCII file.

3. Normalisation of Arterial Input to Allow Comparison of Serial Measurements

In cases where arterial concentrations are not known in the units of tissue concentrations, the algorithm includes a method to allow comparison of relative tissue blood flow and tissue blood volume in serial examinations in the same subject or animal. In order to achieve this, the area of the arterial input function (as determined by gamma variate fitting above) is normalised to the injected dose per body weight prior to the deconvolution below. Likewise, subsequent blood volume measurements are normalised to the aforementioned, dose-normalised arterial input area.

4. Determination of Blood Volume

Using known tracer kinetic principles, relative blood volume is determined as the area under the tissue concentration time curve corresponding to the first-pass of the injected tracer or contrast agent (See e.g. Figure 2 in Example 1), normalised to the arterial input area determined in 3. The area is determined both by direct, numerical integration, and by gamma variate fitting (See section 2).

5. Determination of Blood Flow and Mean Transit Time

Tissue flow, F_t, is determined as the solution to the equation

$$C_t(t) = F_t \cdot C_a(t) \otimes R(t) \qquad \text{Eq. 4}$$

where ⊗ denotes convolution, $C_a(t)$ is the arterial concentration as a function of time, and R(t) is the *residue function*, describing the fraction of particles still present in the vasculature at time t after a unit impulse input.

Mean Transit time (MTT) is given from the blood volume (V) and F_t the central volume theorem

$$MTT = \frac{V}{F_t} \qquad \text{Eq. 5}$$

With tissue and arterial concentrations measured at equidistant time points t_1, $t_2 = t_1 + \Delta t, \ldots, t_N$. Equation 4 can be reformulated as a matrix equation

$$\begin{pmatrix} C_t(t_1) \\ C_t(t_2) \\ .. \\ C_t(t_N) \end{pmatrix} = F_t \cdot \Delta t \begin{pmatrix} C_a(t_1) & 0 & .. & 0 \\ C_a(t_2) & C_a(t_1) & .. & 0 \\ .. & .. & .. & .. \\ C_a(t_N) & C_a(t_{N-1}) & .. & C_a(t_1) \end{pmatrix} \bullet \begin{pmatrix} R(t_1) \\ R(t_2) \\ .. \\ R(t_N) \end{pmatrix}$$

Eq. 6

The equation is (after applying Simpsons rule to the matrix elements (Østergaard 1996b)) solved for $F_t \bullet R(t)$ in each pixel by Singular Value Decomposition (SVD), with a cut-off in diagonal eigenvalues at 20% of the maximum value in order to suppress experimental noise typical of tomographic images (signal to noise ratio of the order of 10). The noise cut-off of 20 % is user specified. In the case of higher signal-to-noise ratio (SNR) or specific SNR characteristics, a Monte Carlo simulation scheme is provided to optimise the cut-off (Østergaard 1996b).

The algorithm allows independent correction for tracer arrival delays prior to deconvolution by shifting the tissue curve in a given pixel by the delay fitted in 2.a.,

thereby reducing bias in flow rates due to simple delays of the tissue curve relative to the arterial input curve (Østergaard 1996a).

The algorithm calculates the following quantities, and stores them as digital, floating point images:

(a) Tissue blood volume (As determined section 2.a. and 4).

(b) Tissue blood volume (As determined by simple, numerical integration up to tracer re-circulation – section 4).

(c) Blood mean transit time determined as the area under the residue function response R(t).

(d) Relative or absolute tissue flow as determined by the maximum value of the impulse response function ($F_t \cdot R(t)$) – Section 5. Here, relative flow, F_r, means a value proportional to (by the same factor throughout the digitised images of relative flows) absolute flow in cases where absolute arterial flow values cannot be determined. Again, absolute flow refers to cases where arterial concentrations are known in the units of the tissue concentration data.

(e) Relative or absolute tissue flow as determined by Equation 5., using the blood volume determined in (b) divided by the MTT determined in (c). Here, relative flow means a value proportional to (by the same factor throughout the digitised images of relative flows) absolute flow in cases where absolute arterial flow values cannot be determined. As above, an absolute flow refers to the cases where arterial concentrations are known in the units of the tissue data.

(f) MTT determined as tissue blood volume (b) divided by tissue flow (d) (Equation 6).

(g) The tissue residue function, R(t).

(h) The goodness of fit, χ^2, of Equation 4 to the tissue concentration time curve.

6. Absolute Quantification

To allow absolute quantification of cerebral blood flow (CBF; ml/100ml/min) or cerebral blood volume (CBV; ml/100ml) measurements with Gd-chelates and dynamic T_2 weighted susceptibility contrast agents values are determined as

$$CBF = 0.87 \cdot B_0 \cdot F, \text{ (humans)}$$

$$CBV = 0.87 \cdot B_0 \cdot V, \text{ (humans)}$$

$$CBF = 1.09 \cdot B_0 \cdot F, \text{ (porcine data)}$$

$$CBV = 1.09 \cdot B_0 \cdot V, \text{ (porcine data)}$$

Where B_0 is the field strength of the magnet in Tesla, and V, and F, are the relative volumes and flows determined as described in section 4 and 5, respectively, where impulse response height and tissue curve area have been appropriately normalised to the arterial input area.

7. Determining the Distribution of Transit Times

To determine the distribution of tissue transit times, h(t), the negative slope of the tissue response is determined in each point as the average of slopes of straight lines connecting the previous and following point on the R(t) curve (See Equation 13 and Equation 14).

Special cases:

7.a. At the initial point of R(t), where only one slope can be defined, the slope of the straight line connecting the initial and second measurement of R(t) is chosen

7.b. In cases where, due to noise, R(t) between to points deviates from being either constant or decreasing as a function of time, the slope is set to zero.

The resulting curve, with the time axis normalised to the mean transit time, is illustrated in Example 2 (Østergaard 1998a).

8. Determining the Distribution of Relative Flows.

In the remainder of the description, relative flows refer to a defined fraction of the mean flow, i.e. a dimensionless quantity, independent of any absolute quantification of flow.

Under the assumption of equal lengths of capillary paths, the distribution of transit times can be converted into a distribution w(f) of relative flows f (i.e. flows normalised such that the mean of the distribution is 1) by the relation

$$f \cdot F_t = \frac{V}{t} \qquad \text{Eq. 7}$$

where V is the associated blood volume (Units of V and F_t may here be arbitrary due to the normalisation in Equation 9), and thereby

$$w(f) = -\frac{t}{f} \cdot h(t) \qquad \text{Eq. 8}$$

where t is a given transit time in the distribution above, h(t) the corresponding negative slope of R(t) and dt is given by the time resolution of the measurements (and thereby R(t)).

Its is finally required that the resulting curve w(f) be a probability density function (PDF), i.e. has area 1, and has mean value 1 (i.e. describes flows relative to total flow), i.e.

$$\int_0^\infty w(f) f df = \int_0^\infty w(f) df = 1 \qquad \text{Eq. 9}$$

This is achieved by iteration, numerically integrating the expressions of w(f) and f above, in each step scaling f and w(f) by the preceding integral.

9. Determining Abnormal Flow Distributions

The resulting distribution of relative flows is recalculated by linear interpolation to determine its values at predefined relative flow values previously determined for normal tissue (Figure 4b in Example 1).

The values read

TABLE 1

f	w(f)	f	w(f)
3.8053	1.65E-03	0.6941	1.4594
2.865	0.0226	0.647	1.5915
2.3306	0.0372	0.6205	1.6279
1.7879	0.0627	0.5969	1.5812
1.5881	0.1198	0.5815	1.351
1.4459	0.1751	0.565	1.3393
1.3535	0.2491	0.5448	1.2367
1.2785	0.3303	0.5262	1.1433
1.1912	0.4058	0.5133	1.0688
1.1106	0.4793	0.5007	0.928
1.0474	0.646	0.4822	0.6559
0.9972	0.7218	0.4689	0.6366
0.9438	0.9032	0.4571	0.4282
0.8981	0.986	0.4416	0.3133
0.8214	1.1098	0.4316	0.0244
0.7794	1.3562	0.42	0

In each image element, the distribution is compared to this standard curve by means of a nonparametric Kolmogorov Smirnov (KS) test, and the corresponding p value is calculated.

The program returns digitized images of

8.a. The KS probability p as a quantitative measure of deviation from the normal distribution.

8.b. 20 images containing the values of w(f) at the predefined values f in Table 1.

8.c. With a specified option, corresponding comparison of the distribution of is performed (with the curve in Figure 4a in Example 1), and the transit times or relative transit times displayed.

10. Absolute Quantification of Flow heterogeneity and Solute Extraction

With a specified option, for susceptibility contrast MR imaging, the program combines the relative flow heterogeneity w(f) with absolute flow estimates (See Section 5) to calculates distribution of absolute flows in ml/100ml/min. Furthermore, using the microvascular weighting (For example as demonstrated in Østergaard 1998c) and table values for the microvascular dimensions of the organ in question (for brain capillaries e.g. 8 μm diameter and 120 μm length), blood volume is converted into capillary surface area, S. The local extraction E of a substance with capillary permeability P (as given by literature values), is then given by:

$$E = \int_0^\infty w(f)\left(1 - e^{-\frac{PS}{f \cdot R}}\right) df \qquad \text{Eq. 10}$$

This quantity is visualised as a separate image, based on the specified value of P. In cases where tomographic images do not possess a specific microvascular weighting, S can be inferred from the blood volume by literature values describing microvascular dimensions and fractions for the relevant organ.

EXAMPLE 1.

MODELING CEREBRAL BLOOD FLOW AND FLOW HETEROGENEITY FROM MAGNETIC RESONANCE RESIDUE DATA

SUMMARY OF THE EXAMPLE

Existing model-free approaches to determine cerebral blood flow by external residue detection show a marked dependence of flow estimates on tracer arrival delays and dispersion. In theory, this dependence can be circumvented by applying a specific model of vascular transport and tissue flow heterogeneity. A method is presented to determine flow heterogeneity by MR residue detection of a plasma marker. Probability density functions of relative flows measured in 6 healthy volunteers were similar among tissue types and volunteers, and were in qualitative agreement with literature measurements of capillary red blood cell and plasma velocities. Combining the measured flow distribution with a model of vascular transport yielded excellent model fits to experimental residue data. Fitted gray:white flow rate ratios were in good agreement with PET literature values, as well as a model-free singular value decomposition (SVD) method in the same subjects. The vascular model was found somewhat sensitive to data noise, but showed far less dependence upon vascular delay and dispersion than the model-free SVD approach.

BACKGROUND

A technique to determine cerebral blood flow (CBF) by magnetic resonance (MR) bolus tracking of an intravascular contrast bolus has recently been presented (Østergaard 1996a). By performing non-parametric singular value decomposition (SVD) deconvolution of tissue time concentration curves by a non-invasively determined arterial input function, the algorithm (hereafter referred to as the SVD method) generates pixel-by-pixel maps of CBF (Østergaard 1996a). The SVD method has been demonstrated to yield CBF values in excellent agreement with PET in normal volunteers (Østergaard 1998a), as well as in an animal hypercapnia model (Østergaard 1998b). Although the model-free SVD method offers the advantage of being independent of the underlying vascular structure, the method is somewhat susceptible to dispersion and delay of the measured AIF before it reaches the imaging pixel (Østergaard 1996b). Especially in the setting of major vessel disease, dispersion in the

feeding vessel may be significant relative to tissue tracer retention, causing underestimation of CBF, and therefore overestimation of the CBV:CBF ratio(Østergaard 1996b). This ratio, the plasma mean transit time (MTT), is an important parameter in evaluating cerebrovascular perfusion reserve, and therefore the inability of the SVD approach to distinguish vascular dispersion from prolonged tissue MTT may ultimately impair its clinical use.

Bassingthwaighte and co-workers have developed modelling tools to describe major vessel transport as well as microvascular tracer retention (King 1993; King 1996). A derived model of the coronary circulation has been successfully applied to MR data, allowing non-invasive measurements of coronary blood flow (Kroll 1996). This model (hereafter referred to as the vascular model), modified for the cerebral circulation, may ultimately provide estimates of CBF and MTT independent of major vessel delay and dispersion. The aim of this study was to extend this vascular model to the cerebral circulation. First, a first-order expression of flow heterogeneity in the cerebral circulation was derived by a model-free analysis of tracer retention in areas of negligible major vessel dispersion. To validate the model, the vascular model was fitted with measured flow heterogeneity to human MR residue measurements, and compare the resulting flow rates to literature values, as well as the SVD method. Finally, the sensitivity of the vascular model to tracer delays was compared in simulated data.

THEORY

Vascular model

A modified version of the vascular model previously described by Kroll et al (Kroll 1996) was used. The vasculature was modelled a major, feeding artery in series with 20 small vessels in parallel – See Figure 1. In the vascular model the flow is directed along the parallel pathways, with w_i representing the fraction of flows with values $f_i \cdot Fp$, where F_p is total flow. The feeding artery was described by a fixed, relative dispersion in transit times (RD = 0.48) and a delay, determined by its volume fraction, V_{art} (King 1993). The capillaries were modelled as simple delay lines of fixed length (100 μm), with volume V_p. In the following, the tissue flow F_p, the feeding vascular volume V_{art}, and capillary volume V_p was allowed to vary. The observed signal changes due to magnetic susceptibility contrast agent arises – when using a spin echo

sequence (See Materials and Methods below) - mainly from capillaries (Fisel 1991; Boxerman 1995; Weisskoff 1994). In the model, total tissue tracer concentrations were therefore calculated based on the amount of tracer in the small, parallel vessels. The distribution of transit times in the capillary bed was incorporated by an algorithm assigning appropriate flows and weights to the parallel vascular paths, to achieve a given heterogeneity (King 1996). This flow heterogeneity is described by a probability density function (PDF), assigning a probability w(f) to a given relative flow f, i.e. flow relative to the mean flow, F_p. In the following, it is described how an estimate of flow heterogeneity in humans is obtained from MR residue data. For a more detailed discussion of modelling flow heterogenity, see King *et al.* (King 1996).

Flow Heterogeneity from Residue Data

The fact that the impulse response to a plasma tracer can be estimated by nonparametric deconvolution of the tissue residue during the tracer passage by a non-invasively determined arterial input function (AIF) is utilised. From this the distribution of plasma transit times, and - under certain assumptions regarding the distribution of capillary lengths – the distribution of flows in the region are derived.

The tissue concentration $C_t(t)$ of tracer in response to an arterial input function $C_a(t)$ is given in Equation 4. The formula is equivalent to the integral

$$C_t(t) = F_t \cdot C_a(t) \otimes R(t) = F_t \cdot \int_0^t C_a(\tau) R(t-\tau) d\tau$$

Eq. 11

where F_t is tissue flow and R is the *residue function*, i.e. the fraction of tracer present in the vasculature at time t after a perfect, infinitely sharp input in the feeding vessel. Assuming the arterial and cerebral concentrations are measured at equally spaced time-points $t_1, t_2, \ldots, t_N$, this equation can be discretized, assuming that over short time intervals Δt, the residue function and arterial input values are constant in time:

$$C_t(t_j) = F_t \cdot \int_0^{t_j} C_a(\tau) R(t-\tau) d\tau \approx \Delta t \cdot F_t \cdot \sum_{i=0}^{j} C_a(t_i) R(t_j - t_i)$$

Eq. 12

which is equal to the expression in Equation 6.

As previously described (Østergaard 1996b), this equation can be modified to residue and arterial input functions that vary linearly in time. The SVD approach provides a powerful numerical tool to solve Equation 6 in the presence of experimental noise to yield the residue function. The distribution of transit times, h(t), is then found from

$$R(t) = \left[1 - \int_0^t h(\tau)d\tau\right] \Rightarrow h(t) = -\frac{dR}{dt}$$

Eq. 13

I.e. the slope of the residue function. At a given time point t_i, h(t) can be estimated as

$$h(t_i) = \frac{1}{2} \cdot \left(\frac{R(t_{i-1}) - R(t_{i-1})}{\Delta t}\right)$$

Eq. 14

The probability density function (PDF) of transit times (t) is turned into a distribution of relative flow rates f, w(f), by requiring

$$w(f)df = h(t)dt$$

Eq. 15

and that the central volume theorem (Stewart 1894) is obeyed (Equation 7). Assuming all vascular paths have equal volume, the distribution of flow rates is obtained from Equation 8, and normalised to have unit mean flow and area (Equation 9).

MATERIALS AND METHODS

Volunteer Data

Six normal volunteers (Age 29 ± 4 yrs) were examined according to a standard perfusion protocol on a GE Signa 1.5 T imager (General Electric, Waukesha, WI) retrofitted for EPI capabilities (Instascan, Advanced NMR Systems, Wilmington, MA), using spin echo (SE), echo planar imaging (EPI) with a time of repetition (TR) of 1.0

seconds, and a time of echo (TE) of 100 ms. The slice thickness was 5 mm with an in-plane resolution of 1.6 mm by 1.6 mm in a 40 by 20 cm field-of-view (FOV). A total of 52 images were acquired, starting 15 seconds before i.v. injection of 0.3 mmol/kg contrast medium (Dysprosium-diamide, Nycomed Imaging, Oslo, Norway). Intravascular contrast agent concentrations, C(t), were estimated assuming a linear relationship between concentration and change in transverse relaxation rate, ΔR_2 (Villringer 1988; Weisskoff 1994) (Equation 1).

Feeding arterial branches were identified in the image slice as pixels displaying early concentration increase after contrast injection (Porkka 1991). This approach does not determine absolute arterial tracer levels, but provides the shape of the AIF. To standardise the analysis below, the arterial input function was therefore scaled to yield a mean CBV of 3% (Østergaard 1998b). In volunteers, a single arterial input function in the imaging plane was used for all tissue regions.

Determination of Flow Heterogeneity

Tissue concentration time curves were formed using Equation 1. Three gray and two white matter tissue regions consisting of 4 image pixels (0.05 cc) were then chosen, based on cerebral blood volume maps (Rosen 1990). The tissue residue function was calculated by SVD deconvolution of the tissue concentration time curve with the AIF. The resulting residue function was then converted into a probability density function (PDF) of relative flows as described in the Theory section above

Model Analysis

The experimentally determined flow heterogeneity PDF was then entered into the vascular model described above. For sixteen gray and white matter regions (0.25-0.4 cc), F_p, V_p, and V_{art} were adjusted to obtain optimal fits to the corresponding tissue concentration time curves by nonlinear regression analysis (Chan 1993). The initial conditions were $F_p = 40$ ml/100ml/min, $V_p = 2\%$, and $V_{art} = 0.1\%$. The remaining model parameters are given in Figure 1.

Comparison with model-free approach

To compare the flow rates obtained with the vascular model with those of the model-free SVD approach (Østergaard et al. 1996a), the height of the deconvolved tissue response curve ($F_t \cdot R(t_i)$ in Equation 3) was determined for the same regions as used

in the model analysis above. After determining mean white matter flow rate, 9 relative gray:white flow ratios were calculated for each volunteer, and compared with those obtained by the vascular model.

Sensitivity to Tracer Delays

In volunteer 4, each pixel tissue concentration time curve was delayed in steps of 0.25 second by linear interpolation to simulate the effects of tracer arrival delays. The simulated image data were then analysed as described above, and fitted flow rates by the SVD and vascular model approach plotted as a function of delay for comparison.

Sensitivity to Noise and Initial Conditions

To determine the overall sensitivity of parameter estimates with the vascular model to experimental noise, a set of synthetic data sets were generated using the vascular model itself, and two sets of typical values for flow, volume, and feeding artery volume ($F_p = 20$ ml/100 ml/min, $V_p = 2\%$, $V_{art} = 0.5\%$, and $F_p = 50$ ml/100 ml/min, $V_p = 3\%$, $V_{art} = 0.5\%$). These were converted into a MR signal intensity time curve using Equation 1, to generate a typical signal loss (25% for gray matter, equivalent to the higher flow) during a bolus passage. Random gaussian noise was then added, and 'noisy' concentration time curves were again calculated from Equation 1. Simulated SNRs varied from 400 down to 12, the latter being typical for raw, pixel-by-pixel data obtained with perfusion protocols on a clinical MR system. The synthetic curves were analysed using the vascular model, using two different sets of initial conditions. These were chosen to represent two extremes of physiological values: $F_p = 80$ ml/100 ml/min, $V_p = 8\%$, $V_{art} = 1\%$, and $F_p = 20$ ml/100ml/min, $V_p = 2\%$, $V_{art} = 0.1\%$. For each SNR, 24 simulations were performed, and the mean and standard deviations of the fitted model parameters were calculated for further evaluation. The dependency on initial conditions was evaluated by recording the number of simulations where two different initial conditions caused resulting fitted parameters to differ by more than 10% from their mean. To compare stability of the vascular model and SVD method to experimental noise, flow rates were determined from the same synthetic curves by the SVD method.

RESULTS

Figure 2 shows a set of typical tissue and arterial concentration time curves obtained from volunteer 1. The tissue ROIs consisted of 25-35 pixels (corresponding to 0.3 - 0.4 cc volumes). The average signal to noise ratio (SNR) (defined as the maximum tissue R_2 increase during bolus passage divided by the standard deviation of the noise relative to pre-bolus base-line image intensity) for the tissue volumes used for model validation (0.25-0.4 cc) was 30. The SNR of gray matter was a factor of 2 to 3 higher than that of white matter, due to the higher blood volume.

Flow heterogeneity

Figure 3 shows the location and size of three regions chosen for determination of flow heterogeneity in volunteer 4. The regions are overlaid on a CBF map calculated by the SVD-method to illustrate the contrast and spatial resolution of the techniques. Also shown are the corresponding flow heterogeneity plots derived from the three regions. The transit time and derived flow heterogeneity PDFs were found to be remarkably similar among regions and among volunteers. Figure 4a shows all pairs of relative transit time t and corresponding h(t) measured for all regions in all 8 volunteers. Figure 4b shows - under the assumption of equal capillary lengths – the corresponding plot of relative flow f and w(f) measured for all regions and volunteers. Due to this constancy across regions and subjects, the (f,w(f)) points were consequently averaged into 30 points (Full curve) and used as a global expression for flow heterogeneity in normal tissue in the subsequent model analysis. The parameterised w(f) is given in Table 1. The distribution of flows is markedly right-skewed, with the majority of capillaries having flow rates less than the mean flow. The maximum probability is reached at roughly 2/3 of the mean flow.

Model validation

In the following, the experimentally determined flow heterogeneity PDF was applied, and the vascular transport is therefore described by only three parameters, V_{art}, F_p and V_p. Figure 5 shows a typical set of tissue concentration time curves as well as the fits provided by the model (Basal ganglia: CBF = 60.3±1.0 (SE) ml/100ml/min, Gray matter: CBF = 48.5±1.2 ml/100ml/min, white matter: CBF = 19.5±0.8 ml/100ml/min). Notice the model takes into account the observed earlier tracer arrival in tissue with higher flow rates. The quality of model fits to experimental data shown in Figure 5 is

typical for the patients examined. Table 2 shows the mean gray:white matter flow ratios for 8 regions. The mean gray:white flow ratio was 2.89±0.35 with the vascular model.

TABLE 2. Regional gray:white flow ratios in 6 volunteers

		Volunteer no.						
Region		1	2	3	4	5	6	Average
Basal ganglia	left	4.19	3.41	3.70	2.73	3.76	3.39	3.53
	right	3.76	3.41	2.99	2.80	3.66	3.86	3.41
Frontal medial	left	2.89	2.91	1.94	2.32	2.55	2.03	2.44
	right	2.66	2.73	3.6	2.24	3.06	3.03	2.88
Temporal	left	3.55	3.16	3.14	2.55	4.31	2.29	3.16
	right	4.52	3.59	3.27	2.02	3.71	2.78	3.31
Occ.-temporal	left	2.50	2.37	2.66	2.20	2.55	2.74	2.50
	right	2.78	2.05	3.70	2.08	1.70	1.97	2.38
Occ. medial	left	3.60	2.87	2.27	2.06	2.30	2.84	2.66
	right	2.95	2.12	3.57	2.17	2.15	2.43	2.57
Average		3.34	2.86	3.08	2.31	2.97	2.74	2.89

Comparison with model-free approach

Figure 6 shows gray:white matter flow ratios determined by the model approach plotted versus corresponding ratios in identical regions determined by the SVD approach. The three volunteers were chosen based on a significant spread in individual, regional gray:white matter ratios, in order to facilitate comparison between approaches. In the figure, linear regression lines for each volunteer are shown (Volunteer 1: $y = 1.02 + 0.21$ ($r^2 = 0.75$), Volunteer 2: $y = 1.16x - 0.68$ ($r^2 = 0.91$), Volunteer 6: $y = 0.95x - 0.72$ ($r^2 = 0.95$)). The line of identity was within the 95%

confidence intervals of a common linear fit. Notice regional gray:white matter ratios using the two techniques all lie near the line of identity.

Sensitivity to tracer arrival delays

Figure 7a shows the effect of AIF delay on fitted flow rates for the vascular model and the SVD approach, respectively. The gray and white matter tissue ROIs consisted of 90 image pixels (1.1 cc). Vascular model and SVD values were obtained from identical regions. The SVD approach progressively underestimates flow rates with tracer arrival delay. The relative underestimation is roughly proportional to the delay, reaching 25% for white matter and 35% for gray matter at a delay of 3 seconds, respectively. For the model approach, flow estimates are remarkably independent of delay. Figure 7b shows the fitted feeding artery volume as a function of delay. The vascular model interprets increasing delays as increased feeding vessel volume in accordance with the definition of the vascular operator. As vascular dispersion is *a priori* unknown in actual measurements, fitting was performed assuming a vascular dispersion RD = 0.48, although the delay was simulated to be dispersion-less Notice fluctuations of fitted flow values around 1 is accompanied by fluctuations of the fitted vascular volumes. These fluctuations and the tendency of flow and vascular volume to co-vary are discussed further below.

Sensitivity to noise and initial conditions

Figure 8 shows the means and standard deviations of the fitted flow rates for two sets of simulated data (V_{art} = 0.5%, F_p = 60 ml/100ml/min, V_p = 3%; V_{art} = 0.5%, F_p = 20 ml/100ml/min, V_p = 2%), using the model (Figure 8a) and SVD (Figure 8b) approach, respectively. Raw image data noise was varied from that of typical, clinical data (~12) to 400. The SVD approach overestimates flow rates somewhat for this choice of model parameters, whereas the vascular model fits are roughly equal to the input parameters. The uncertainty (error bars in Figure 8a and 8b indicate one standard deviation, derived from the simulated data) on fitted flow rates display the expected increase as a function of increasing raw image data noise.

For low SNR, error bars are roughly equal in size for the SVD and model approach, respectively. For high SNR, however, the uncertainty on vascular model fits did not reach zero as was the case for the SVD approach. To investigate whether factors

other than noise contributed to the observed behaviour, the dependence of model fits on initial conditions and the tendency of parameters to co-vary was analysed. The fraction of fits, where initial conditions were found to significantly affect the fitted flow rates (defined as cases where two different initial conditions resulted in fitted flows that differed by more than 10% from their mean) was found to be negligible for SNR above 20. For lower SNR, 15-20% of fits gave ambiguous results. Therefore, the standard deviations for the low SNR may be somewhat underestimated due to bias by the choice of initial conditions.

During simulations, fitted feeding artery volumes and fitted tissue flows were found to co-vary: high, fitted flow rates were hence often accompanied by high arterial volumes. Figure 9 shows fitted flow rates versus corresponding fitted feeding artery volumes from simulated curves with SNR = 40. This pattern of co-varying fitted flow rates and feeding artery volumes was found at all noise levels. It was found that varying flow and feeding artery volume in proportion lead to only small changes in the shape of the resulting concentration time curve. Therefore, the presence of modest experimental noise leads to relatively large uncertainties in fitted flow rates. This is thought to explain the unexpected, large standard deviation of flow estimates at high SNR for the vascular model, as well as the fluctuations around unit relative flow in Figure 7.

DISCUSSION

Overall validity of model

The vascular model, after incorporation of the experimentally determined heterogeneity PDF, provided excellent fits to the experimental data. The model fits of CBF yielded a mean gray:white flow ratio of 2.8±0.35, in agreement with the PET literature ratio of 2.65 for subjects of similar age (Leenders 1990). The ratios were also in good agreement with those found using the model-free approach. In contrast to the SVD approach, the model approach provided fits to experimental data that were essentially independent of vascular delay. The model was simplified considerably by the use of one flow heterogeneity PDF for all types of tissue. By characterising the model by only three parameters, a remarkable stability of the model was obtained, even compared to the pixel-by-pixel based SVD approach. Co-varying vascular volume and flow rate in model fits to low SNR data was found to be a major contributor to

uncertainty in model fits of CBF. Below, the individual elements of the model are discussed in further detail.

Model considerations

The model presented here differs slightly from that previously described by Kroll *et al.* (Kroll 1996) in the heart. Kroll *et al.* (Kroll 1996) described the arteriolar and capillary compartments separately, assigning fixed relative dispersion and variable volumes to the arteriolar vascular paths, and a fixed volume to the capillary bed. In the brain, capillary density varies greatly among different tissue types. For the purpose of obtaining a robust model for all types of brain tissue with the same choice of basic model parameters, the microvascular volume was kept as a free parameter. In terms of vascular transport, the models are similar, except that in the model presented here, dispersion takes place only in the large vessel, whereas small vessel dispersion is accounted for by the flow heterogeneity PDF. Despite the simplification of the model, it is likely that, by limiting the number of vascular elements and thereby the number of free parameters, the stability of the model to noise has increased significantly, as outlined in the analysis above. The robustness of the model to experimental noise is imperative to ultimately study CBF at high spatial resolution. Kroll *et al.* assumed that only small vessel tracer levels are observed by the residue detection (Kroll 1996). Here, this assumption is further justified by the inherent sensitivity of susceptibility contrast to microvessels (Fisel 1991; Weisskoff 1994; Boxerman 1995).

Vascular transport and dispersion term

As discussed elsewhere (Østergaard 1996b), nonparametric deconvolution approaches do not allow separation of macrovascular transport and microvascular retention. Therefore, modelling vascular retention is necessary, whenever vascular transport significantly changes the input bolus shape upstream of the AIF measurement site. The vascular transport operator model used in the present model is generally accepted for modelling normal major vessel transport. The advantage of including vascular transport in the kinetic modelling is demonstrated in Figure 5: The fact that tracer arrives earlier in tissue with high flow rate due to a faster feeding vessel transit is accounted for by the model approach, unlike the model-free SVD approach. The difficulty in introducing this operator lies mainly in the fact that the transfer functions of the major vessel and the microvascular network are very similar. This, in turn, leads

to the difficulty in separating vascular volume and flow, as observed in the simulations (Figure 9). The analysis presented here also suggest that this effect contributes significantly to the uncertainty of flow estimates, even at modest noise levels, just at it may play a role in the dependency upon initial conditions of fitted flow rates. These findings are in agreement with those previously reported by Kroll *et al* (Kroll 1996). In cerebrovascular diseases, blood may pass through stenoses with marked turbulence, or through irregular collateral paths upstream of the arterial sampling site. In these cases, the vascular operator may not be adequate, and the vascular transport function should ideally be measured independently. Indeed, novel MR techniques detecting the inflow of spin labelled arterial blood to a given brain region may ultimately provide this information (Wong 1997). Such independent measurements would serve to avoid the interdependence of flow and vascular volumes using vascular models, or alternatively allow application of the model-free SVD approach. In severe cases, however, vascular dispersion may dominate total tracer retention, in which case estimates of flow rate by residue detection of an intravascular tracer become uncertain (Østergaard 1996b; Kroll 1996).

Flow heterogeneity

Reports of cerebral flow heterogeneity are mainly based on invasive measurements of plasma or red blood cell velocities in rats. Abounader *et al.* utilized bolus injection of a plasma marker followed by decapitation, deriving plasma flow velocity from capillary filling in histology (Abounader 1995). Hudetz *et al* determined the frequency of red blood cell (RBC) velocities in capillaries using intravital video microscopy (Hudetz 1997). Both found the distribution of blood elements to be very heterogeneous, with a right-skewed shape. Figure 10 shows their findings along with the PDF determined here. The data of Hudetz *et al* (Hudetz 1997) were normalised as the relative flow PDF (See Theory, Equation 9). From the data of Abounader *et al.* (Abounader 1995), a normo-capnic data set was chosen, and axes scaled to facilitate comparison with the other curves (plasma flow units did not allow direct normalisation). It should be noticed that these measurements are not directly comparable. First, plasma and RBCs follow different paths through the capillary network, so the measurements presented here should be more comparable to the plasma velocity measurements. Secondly, the flow distribution curve derived in this study assumes equal capillary lengths. Although the relationship between capillary plasma flow and flow velocity is a complex function

of capillary length and architecture, a finite distribution of capillary lengths is likely to result in blood velocities being more dispersed than relative capillary flows (As seen when comparing the PDF presented here with the RBC velocity study). The similarity of the present measurements with these independent, invasive methods lends hope to the use of this approach in describing normal microvascular dynamics. In altered physiological states or disease, the flow heterogeneity may not be as constant among tissue types as found in this study. Abounader *et al.* (Abounader 1995) determined the heterogeneity of microvascular flow at different degrees of hypercapnia, and found that plasma flow became more homogenous at higher flows. A similar finding for red blood cell velocities was reported by Hudetz *et al.* (Hudetz 1997). This could be the case in disease as well, and caution should therefore be exercised in choosing flow heterogeneity PDF for use with vascular models in these cases. The model-free approach to determine flow heterogeneity PDF presented here may provide insight with respect to the distribution of relative flows in these cases. Using this approach, it should be kept in mind solving Equation 1 belongs to a class of so-called inverse problem, meaning that any noise in measured tissue concentrations may lead to large changes in the resulting residue function. As suppression of noise inevitably causes loss of underlying information, the SVD deconvolution therefore may not yield the exact shape of the underlying residue function. Likewise, one may not be able to distinguish slightly different flow heterogeneity PDF based on noisy measured concentration time curves. Although the flow heterogeneity PDF and derived flow rates were found in agreement with independent findings, it is therefore important to further validate the approach presented here.

Utility of vascular models

Although cerebral blood flow itself is an important index of brain function, the heterogeneity of microvascular flow and transit times described here may be a more important determinant of cerebral metabolism. As discussed by Kuschinsky *et al.*, the degree of heterogeneity among capillary paths determines the net capillary-to-tissue concentration gradients necessary to drive delivery of nutrients (Kuschinsky et al., 1992). Indeed, regulation of capillary flow heterogeneity may play a major role in the brains ability to increase e.g. oxygen delivery to meet cellular metabolic demands (Kuschinsky et al., 1992). This issue can be addresses in great detail by combining flow heterogeneity measurements with spatially distributed models of oxygen

exchange (Li 1997). The analysis presented here, combined with these models, may ultimately lead to a more extensive understanding of, for example, the fundamental limitations of oxygen delivery in stroke, where the survival of tissue may partially depend on the ability to increase oxygen extraction by an increased mean transit time. Also, modelling the exact relationship between cellular oxygen consumption and vascular oxygen levels may facilitate a quantitative metabolic interpretation of deoxyhemoglobin concentration changes observed by functional magnetic resonance imaging (Kwong 1992).

EXAMPLE 2.

MAGNETIC RESONANCE IMAGING MEASUREMENTS OF FLOW HETEROGENEITY DEMONSTRATE HIGH RISK OF INFARCTION IN ACUTE STROKE

SUMMARY OF THE EXAMPLE

The ability of brain tissue to survive ischemic episodes is believed to be related to changes in the dynamics of capillary blood flow. Using a novel magnetic resonance imaging based method to measure microvascular transit time dynamics, the flow heterogeneity and tissue mean plasma transit times was examined in 11 patients presenting with acute (<12 hours after symptom onset) stroke. In normal brain tissue, the distribution of relative flows was found to be markedly skewed towards high capillary flow velocities. Within regions of decreased cerebral blood flow, plasma mean transit times were prolonged. Furthermore, subregions were identified with significant loss of the high-flow component of the flow distribution, thereby causing increased homogeneity of flow velocities. These findings are in agreement with independent, invasive measurements of flow heterogeneity in states of decreased perfusion pressure in animal models. In parametric maps quantifying the acute deviation of flow heterogeneity from that of normal tissue, areas of extreme homogenisation of capillary flows predicted final infarct size on follow-up scans in 10 out of 11 patients. Flow heterogeneity and plasma mean transit time can be rapidly assessed as part of a routine clinical magnetic resonance examination, and may provide a tool for individual planning of stroke treatment, as well as in targeting and evaluating emerging therapeutic strategies.

BACKGROUND

Acute stroke is the third leading cause of death, and the leading cause of adult disability. Emerging therapeutic strategies seek to minimise the progression of tissue damage in the acute phase of the disease. Methods to rapidly assess the severity and later progression of acute stroke in individual patients are therefore highly desirable to plan individual treatment, as well as to evaluate novel therapeutic strategies.

In acute cerebral ischemia, delivery of nutrients is severely compromised, and tissue survival therefore depends on tissue regulatory mechanisms to meet metabolic needs. Studies using positron emission tomography (PET) have shown that mean blood transit

time (MTT) and, with further drop in cerebral perfusion pressure, also the oxygen extraction fraction (OEF) are increased in 'tissue at risk' of infarction (Gibbs 1984; Baron 1981). Although the relationship between prolonged blood MTT and OEF remains unclear, both phenomena are believed to reflect underlying regulatory mechanisms attempting to compensate for a decrease in perfusion pressure.

One mechanism for vasoregulatory control is believed to be the ability to alter the *heterogeneity* of blood transit times and thereby the mean capillary concentration of substances diffusing from blood to tissue (Kuschinsky and Paulson 1992). Animal experiments in rats have revealed decreased flow heterogeneity during whisker-barrel stimulation(Vogel and Kuschinsky 1996), indicating that this may be the mechanism underlying the normal brain's striking ability to meet increased metabolic needs during functional activation. Furthermore, Hudetz *et al.* demonstrated that graded decrease in perfusion pressure causes progressive loss of high-flow components, thereby decreasing total flow heterogeneity(Hudetz 1996). Decreasing flow heterogeneity therefore seems to play a crucial role in maintaining sufficient concentration gradients to drive diffusion of nutrients such as oxygen from blood into the cells (Kuschinsky and Paulson 1992). This suggests that blood mean transit time *and* the degree of flow heterogeneity are important indices to assess and further understand the ability of the brain to survive ischemic episodes.

The heterogeneity of flows in normal volunteers by magnetic resonance imaging (MRI) residue detection has recently been studied (Østergaard 1999). It was found that the probability density function (PDF) of relative flows was remarkably constant within and among normal volunteers. In this study, magnetic resonance residue detection was used to study plasma mean transit times as well as flow heterogeneity patterns in patients presenting with acute stroke. Furthermore, these findings were correlated with later neuronal death by comparing initial diffusion weighted imaging (DWI) with follow-up MRI or computed tomography (CT).

The present findings show that flow heterogeneity changes, previously only detectable by invasive microscopy in animal models, can be assessed by a 2-minute examination as part of routine MRI of acute stroke patients. Furthermore, the degree of heterogeneity change relative to normal tissue is a powerful predictor of later

neuronal death, suggesting flow heterogeneity may provide an important diagnostic tool in stroke patient management.

MATERIALS AND METHODS

Patient data

All patients were treated with best medical management, but did not receive tPA or other thrombolytic traeatment. DWI and CBF results for these patients are reported earlier(Sorensen 1998).

Imaging was performed on a GE Signa 1.5 T imager (General Electric, Waukesha, WI) retrofitted for EPI capabilities (Instascan, Advanced NMR Systems, Wilmington, MA).

MRI Perfusion Protocol. Determination of CBV, CBF, MTT, and flow heterogeneity. Perfusion imaging was performed using spin echo (SE) or gradient echo (GE), echo planar imaging (EPI) with a time of repetition (TR) of 1.5 seconds, and a time of echo (TE) of 100 ms (50 ms for GE EPI). The slice thickness was 5 mm with an in-plane resolution of 1.56 mm by 1.56 mm in a 40 by 20 cm field-of-view (FOV). A total of 52 images were acquired, starting 15 seconds before i.v. injection of 0.2 (SE-EPI) or 0.1 (GE-EPI) mmol/kg Gd-based contrast agent. Intravascular contrast agent concentrations, C(t), were quantified assuming a linear relationship between concentration and change in transverse relaxation rate, ΔR_2 (Villringer 1988; Weisskoff 1994). The shape of the arterial input function (AIF) was determined from feeding arterial branches, identified in the image slice as pixels displaying early concentration increase after contrast injection (Porkka 1991). The tissue residue function (or impulse response function) was calculated by deconvolving the tissue concentration time curve by the AIF, using singular value decomposition (SVD) (Østergaard 1996a; Østergaard 1996b). CBF was determined as the height of the deconvolved tissue curve. CBV was determined by the area under the tissue concentration time curve, as previously described (Rosen 1990), and the plasma mean transit time (MTT) formed as the ratio CBV/CBF(Stewart 1894). Finally, the distribution of tissue transit times *in each imaging voxel* was determined as the slope of the residue function, and by assuming equal lengths of capillary paths, the corresponding probability density function (PDF) of relative flows was determined by means of the central volume theorem(Stewart 1894; Østergaard 1999). In order to quantify and compare the

deviation of the experimentally determined PDF from that found in normal brain, a Kolmogorov-Smirnov test was performed, comparing the flow PDF in a given pixel to that previously determined in normal tissue (See Results, Figures 11a, 11b and 11c) (Press 1992; Østergaard 1999). The corresponding p-value (Null-hypothesis: flow heterogeneity distribution is equal to that of normal tissue) was considered statistically significant if $p<0.01$ (Without Bonferoni correction).

Initial and final infarct sizes.

At the initial scan, infarct size was assessed by diffusion weighted imaging (DWI) (Moseley 1990), acquired using EPI and b-values ranging from 892-1221 s/mm^2. Measurements were performed in 17-20 slices to cover the whole brain. Final infarct size was assessed from DWI images acquired 2-5 days after the infarct, from T_2 or FLAIR MR images acquired at least 5 days after the infarct, or from CT images acquired more than 5 days after the infarct if no MRI was available.

Volumetric Analysis

Using a semi-automatic image analysis software package (ALICE, Hayden Image Processing Group, Boulder, CO) initial and final infarct volumes were calculated based on initial DWI and follow up studies, respectively. In addition, volumes of prolonged MTT and abnormal p ($p<0.01$) were defined, in order to assess the ability of combined DWI and MTT, respectively p-maps to predict final infarct volumes.

RESULTS

Eleven hyperacute stroke patients, 7 male and 4 female, with mean age 61 (range 33-80) years, were examined within 12 hours of symptom onset (Table 3). All patients showed diffusion abnormalities on the initial DWI (Moseley 1990), consistent with ischemic neuronal death prior to the initial scan. Furthermore, all patients showed greater volumes of decreased cerebral blood flow (CBF) and/or increased MTT in the hemisphere of infarction.

TABLE 3

Patient	Age/sex	Hours
1	33 M	4.5
2	78 F	3
3	55 M	2
4	53 M	3
5	72 F	2.5
6	64 F	5.5
7	79 M	7.0
8	80 F	11.0
9	45 M	4.0
10	65 M	11.5
11	45 M	6.5

Age, sex, time of initial MRI for 11 acute stroke patients. Patient 9 showed spontaneous reperfusion of the occluded vessel on the follow-up MR angiography.

Flow heterogeneity findings

Outside volumes of prolonged MTT, the shape of the tissue flow PDF was similar to that previously found in normal volunteers, namely a right-skewed distribution with a distinct distribution of high flow rates. Inside volumes of prolonged mean transit times, the shape of the flow PDF was either like that of normal tissue, or showed distinctive loss of the high-flow portion of the PDF: To illustrate the first type, Figures 11a, 11b, and 11c show a typical pattern in patient 6. This patient, a 64 year old female, was examined 5.5 hours after onset of left leg weakness, and showed prolonged MTT corresponding to the anterior cerebral artery territory (Figure 11a). Figure 11b shows the flow heterogeneity plots for normal brain tissue as well as two regions of prolonged mean transit time (Areas are indicated on the MTT map with numbers corresponding to the PDF curves). The flow PDF in normal tissue was markedly right-skewed, and matched the shape previously found in normal volunteers (Østergaard 1999). The volumes of increased MTT displayed PDFs with a more symmetric shape, with a tendency to loose the high-flow population found in normal

tissue. The degree of symmetry varied within the volume of increased MTT. The deviation from the normal PDF was subsequently quantified by a Kolmogorov-Smirnov test, yielding the probability p that the curve belong to the distribution of relative flows of normal tissue (from ref (Østergaard 1999)). In figure 11c, areas with large deviations of the PDF from that of normal tissue ($p<0.01$) are shown by a colour coded overlay of p onto the acute CBF map. Based on the previous experience (Østergaard 1999) a significance level of $p<0.05$ displays few PDF abnormalities in normal tissue, except in major vessels. Therefore, $p<0.01$ was chosen to highlight highly significant deviations from normal flow heterogeneity PDF.

MTT, flow heterogeneity and later infarction

In 8 out of 11 patients, comparison of initial DWI images with the follow-up study showed that lesion size had increased in between the initial and follow-up scans. In all 8 cases, neuronal death had occurred within the region initially displaying increased MTT. Figures 12a and 12b show this correlation in patient 11, a 45-year-old male 6.5 hours after onset of symptoms. On the initial DWI (first row), cell death is localised to deep gray matter, whereas the acute MTT maps (second row) show prolonged MTT corresponding to the whole middle cerebral artery territory. The p-map shows highly significant deviations from the normal flow PDF in anterior and posterior sub-regions. These subregions corresponded well with tissue that later infarcted, displayed as bright regions in the 2-month follow-up FLAIR MRI images (bottom row). In Figure 13, final infarct volumes are compared to the initial abnormalities of DWI + MTT and DWI + p maps, respectively. Notice the striking ability of combined initial DWI and p-maps to predict final infarct size. In 10 out of 11 patients, p maps (excluding vessels and volumes with preserved, high flow component, see below) corresponded well with the final infarct. Figures 14a and 14b show the respective maps from patient 3. Notice that the initial lesion (top row) and extent of MTT prolongation (second row) are similar to that observed in Figures 12a and 12b. Although the CBF was significantly decreased (Third row, gray scale image), there were only small abnormalities in the flow heterogeneities (indicated by coloured areas on overlay on the CBF map). The small spots correspond to vessels, having a high degree of flow heterogeneity. The final infarct size was similar to that observed on the initial DWI, indicating that the heterogeneity may again have served as a predictor of final outcome.

To demonstrate the predictive value of the p-maps in cases of white matter ischemia, Figures 15a and 15b show maps from patient 8, a 80 year old female. Small infarcted areas are seen on the initial DWI images (Top row). The MTT image shows abnormalities extending into white matter around the initial lesions. Again, flow heterogeneity changes are observed in smaller subregions, corresponding well to the regions that went on to infarction. Notice symmetrically located areas with low p values, corresponding to vessels.

Artifacts in p-maps

In one case, (patient 8), p maps underestimated the final infarct size. Figure 16 shows one slice from this patient, displaying areas with $p<0.1$. Notice high-intensity areas correspond to areas that later infarcted, whereas a number of areas showed unspecific p increase. Separate evaluation of areas with $p<0.01$ would in this patient cause underestimation of final infarct size. Interestingly, follow-up MR angiography in this patient demonstrated spontaneous reperfusion between initial and follow-up scans. In the p-maps, small areas of low p-values were in some cases observed at the location of major vessels (See Figure 12b and 15b), due to the homogenous flow pattern in vessels relative to that in tissue. These areas were not included when defining areas of abnormal tissue flow heterogeneity for comparison with follow-up studies. In patients 3 and 4, areas unrelated to major vessels showed low p-values in a single slice, whereas adjacent tissue in neighbouring slices showed no abnormalities. Analysis of the flow heterogeneity PDF in these single slices revealed a high-flow distribution similar to that of normal tissue, whereas the low-flow component showed flow components down to zero (unlike the relatively sharp cut-off at 0.5 observed in normal tissue - See Figure 11b). This is interpreted as being due to dispersion of the AIF relative to the tissue. Based on the preserved high-flow component and the normal PDF observed in adjacent tissue in neighbouring slices, these areas were not included when comparing p-maps with follow-up images. Below these phenomena are further discussed.

DISCUSSION

The study confirms the report by Hudetz *et al* in animals that decreased perfusion pressure (CBF:CBV ratio) is associated with progressive loss of high-flow

components(Hudetz 1996). The study extends these findings by documenting loss of flow heterogeneity in human acute stroke, and good agreement between heterogeneity changes in early ischemia and eventual tissue infarction. The findings presented hence strongly support the hypothesis by Hudetz *et al* that gradual loss of the high flow component of the flow heterogeneity PDF heralds local loss of functional reserve capacity, and thereby neuronal death (Hudetz 1996). The finding that p-maps predict final infarct size with high certainty in untreated patients suggest that MR heterogeneity measurements may prove useful for individual planning of patient management, as well as for evaluation of new therapeutic approaches in smaller patient populations.

The hypothesis of heterogeneity changes being the driving force in regulating oxygen delivery to tissue (Kuschinsky and Paulson 1992; Vogel and Kuschinsky 1996) suggest a close relationship between the findings presented here and the OEF increase observed by PET in tissue at high risk of subsequent infarction(Powers 1991; Wise 1983). Indeed, qualitative analysis of the kinetics of oxygen delivery show that one should expect reduced heterogeneity of blood flow to produce an increased flow of oxygen into the tissue in states of decreased flow, as illustrated in Figure 17. The curve is a plot of the oxygen flow into tissue versus blood flow. From the convex shape of the curve it can be seen that oxygen flow into the tissue at a given mean blood flow is greater when blood flow is homogenous than when blood flow is more heterogeneous: Oxygen flow into tissue versus blood flow F_t, related through the equation $F_t \cdot (1-e^{-PS/F_t})$, where PS is the permeability to oxygen times the surface area of capillaries (Renkin 1959; Crone 1963). If all blood flow is at the normal mean flow, f_{norm}, the oxygen flow into tissue is given by the height of A. If part of the flow is at f_{low} and the rest at f_{high}, with weightings to maintain the same mean flow, the oxygen flow into the tissue will be the height of D. Notice, as mean flow is reduced and f_{high} and f_{low} changed to maintain the same $CMRO_2$, both f_{low} and f_{high} approach f_{min}, thereby decreasing the degree of heterogeneity. Notice decreased flow heterogeneity with constant flow will increase oxygen delivery, in parallel with the findings of Vogel *et al*, who found decreased heterogeneity in states of functional activation and thereby increased oxygen metabolism(Vogel and Kuschinsky 1996).

The observed shifts toward a homogenous flow distribution may therefore signal increased utilization of metabolic regulatory capacity, explaining the risk of neuronal

death observed in these regions of extreme flow homogenisation. PET is today the method of choice to demonstrate metabolic reserve capacity in cerebrovascular disease. However, future studies should focus on the relationship between MR flow heterogeneity measurements and OEF measured by PET to further explore this coupling of microvascular dynamics and metabolism.

Neuronal death was localised in areas initially displaying prolonged plasma mean-transit times. This is agreement with the previous experience using this technique (Sorensen 1998), as well as studies using PET (Heiss 1994; Baron 1981) and single photon emission computed tomography (SPECT) (Buell 1988). Although the CBV:CBF ratio (i.e. 1/MTT) depends linearity on the cerebral perfusion pressure over a range of values(Schumann 1998), this dependence is likely to be lost when maximum vasodilation is reached at low pressures(Powers 1991). The MTT prolongation may therefore not be directly related to the severity of the perfusion pressure drop and hence risk of infarction. The findings support, however, that prolonged MTT is an early sign of decreased perfusion pressure, at a stage where regulatory mechanisms may still suffice to ensure tissue survival.

Although the high flow component seem crucial to tissue survival, the low flow component of the flow heterogeneity PDF may also prove useful in planning therapeutic approaches. Intravital microscopy studies suggest that maintaining capillary flow velocities above a fixed, lower limit is essential to avoid white blood cell plugging of capillaries(Hudetz 1998; Yamakawa 1987). The distributions of absolute flows in single pixels may prove useful in assessing of leukocyte adhesion prior to therapeutic attempts to reperfuse tissue.

In patients with cerebrovascular disease, the AIF may undergo dispersion and delays upstream of site of measurement, possibly causing overestimation of MTT (Østergaard 1996a; Østergaard 1996b). This bias was reduced by choosing AIFs in the vascular territory affected by the vascular occlusion. Furthermore, dispersion of the AIF will tend to broaden the flow PDF. Therefore, the effects of dispersion *counteract* the observed homogenisation of flow elements. In determining the flow PDF, high p values were observed near vessels (and therefore easily identifiable on the accompanying CBV maps), as major vessel flow inherently homogenous. Probability

maps should therefore be carefully inspected for vessels on CBV maps, as well as signs of vessel dispersion in the PDF shape in a given region. SE-EPI images are particularly suited for this type of analysis, as large vessels are suppressed due to the inherent microvascular weighting of these images (Fisel 1991; Boxerman 1995; Weisskoff 1994).

Given these precautions, the findings presented here indicate that magnetic resonance based assessment of flow heterogeneity provides a powerful tool to study residual metabolic reserve capacity in peri-infarct tissue. Combined conventional MRI, MR angiography, DWI, determination of flow heterogeneity and plasma mean transit time can be performed in roughly 20 minutes on most clinical MR systems. Unlike PET and SPECT, examinations can therefore be performed within the short time-window where treatment should be initiated in order to prevent the progression of neuronal death. Presence of tissue with loss of flow heterogeneity may in the future serve to guide individual patient management, and point to tissue that may serve as target for novel therapeutic approaches.

REFERENCES

Abounader R, Vogel J, Kuschinsky W . 1995. Patterns of capillary plasma perfusion in brains in conscious rats during normocapnia and hypercapnia. Circ.Res. 76:120-6.

Baron JC, Bousser MG, Rey A, Guillard A, Comar D, Castaigne P. 1981. Reversal of focal "misery-perfusion syndrome" by extra-intracranial arterial bypass in hemodynamic cerebral ischemia. A case study with 15O positron emission tomography. Stroke 12:454-9.

Boxerman JL, Hamberg LM, Rosen BR, Weisskoff RM. 1995. MR contrast due to intravascular magnetic susceptibility perturbations. Magn.Reson.Med. 34:555-66.

Buell U, Braun H, Ferbert A, Stirner H, Weiller C, Ringelstein EB. 1988. Combined SPECT imaging of regional cerebral blood flow (99mTc-hexamethyl-propyleneamine oxime, HMPAO) and blood volume (99mTc-RBC) to assess regional cerebral perfusion reserve in patients with cerebrovascular disease. Nuklearmedizin. 27:51-6.

Chan IS, Goldstein AA, Bassingthwaighte JB. 1993. SENSOP: a derivative-free solver for nonlinear least squares with sensitivity scaling. Ann.Biomed.Eng. 21:621-31.

Crone C. 1963. The permeability of capillaries in various organs as determined by use of the indicator diffusion method. Acta Physiol.Scand. 58:292-305.

Fisel CR, Ackerman JL, Buxton RB, Garrido L, Belliveau JW, Rosen BR, Brady TJ. 1991. MR contrast due to microscopically heterogeneous magnetic susceptibility: numerical simulations and applications to cerebral physiology. Magn.Reson.Med. 17:336-47.

Gibbs JM, Wise RJ, Leenders KL, Jones T. 1984. Evaluation of cerebral perfusion reserve in patients with carotid-artery occlusion. Lancet 1:310-4.

Heiss WD, Graf R, Wienhard K, Lottgen J, Saito R, Fujita T, Rosner G, Wagner R. 1994. Dynamic penumbra demonstrated by sequential multitracer PET after middle cerebral artery occlusion in cats. J Cereb.Blood Flow Metab. 14:892-902.

Hudetz AG, Biswal BB, Feher G, Kampine JP. 1997. Effects of hypoxia and hypercapnia on capillary flow velocity in the rat cerebral cortex. Microvasc.Res. 54:35-42.

Hudetz AG, Feher G, Kampine JP. 1996. Heterogeneous autoregulation of cerebrocortical capillary flow: evidence for functional thoroughfare channels? Microvasc.Res. 51:131-6.

King RB, Deussen A, Raymond GM, Bassingthwaighte JB. 1993. A vascular transport operator. Am.J.Physiol. 265:H2196-H2208

King RB, Raymond GM, Bassingthwaighte JB. 1996. Modeling blood flow heterogeneity. Ann.Biomed.Eng. 24:352-72.

Kroll K, Wilke N, Jerosch HM, Wang Y, Zhang Y, Bache RJ, Bassingthwaighte JB. 1996. Modeling regional myocardial flows from residue functions of an intravascular indicator. Am.J.Physiol. 271:H1643-H1655

Kuschinsky W, Paulson OB. 1992. Capillary circulation in the brain. Cerebrovasc.Brain Metab.Rev. 4:261-86.

Kwong KK, Belliveau JW, Chesler DA, Goldberg IE, Weisskoff RM, Poncelet BP, Kennedy DN, Hoppel BE, Cohen MS, Turner R, and others. 1992. Dynamic magnetic resonance imaging of human brain activity during primary sensory stimulation. Proc.Natl.Acad.Sci.U.S.A. 89:5675-9.

Leenders KL, Perani D, Lammertsma AA, Heather JD, Buckingham P, Healy MJ, Gibbs JM, Wise RJ, Hatazawa J, Herold S, and others. 1990. Cerebral blood flow, blood volume and oxygen utilization. Normal values and effect of age. Brain 113:27-47.

Li Z, Yipintsoi T, Bassingthwaighte JB. 1997. Nonlinear model for capillary-tissue oxygen transport and metabolism. Ann.Biomed.Eng. 25:604-19.

Moseley ME, Cohen Y, Mintorovitch J, Chileuitt L, Shimizu H, Kucharczyk J, Wendland MF, Weinstein PR. 1990. Early detection of regional cerebral ischemia in cats: comparison of diffusion- and T2-weighted MRI and spectroscopy. Magn.Reson.Med. 14:330-46.

Porkka, L., Neuder, M. S., Hunter, G., Weisskoff, R. M., Belliveau, J. W., and Rosen, B. R. 1991. Arterial Input Function Measurement with MRI. Proceedings of The Society of Magnetic Resonance in Medicines 10th Annual Meeting 120 p.

Powers WJ. 1991. Cerebral hemodynamics in ischemic cerebrovascular disease. Ann Neurol 29:231-40.

Press WH, Teukolsky SA, Vetterling WT, Flannery BT. 1992. Numerical Recipes in C. The Art of Scientific Computing. Oxford: Cambridge University Press.

Renkin EM. 1959. Exchangeability of tissue potassium in skeletal muscle. Am.J Physiol. 197:1211-5.

Rosen BR, Belliveau JW, Vevea JM, Brady TJ. 1990. Perfusion imaging with NMR contrast agents. Magn.Reson.Med. 14:249-65.

Schumann P, Touzani O, Young AR, Baron JC, Morello R, MacKenzie ET . 1998. Evaluation of the ratio of cerebral blood flow to cerebral blood volume as an index of local cerebral perfusion pressure. Brain 121:1369-79.

Sorensen AG, Copen WA, Østergaard L, Buonanno FS, Gonzalez RG, Rosen BR, Schwamm LH, Weisskoff RM, Koroshetz WJ. 1999. Simultaneous Measurement of Relative Blood Volume, Relative Blood Flow, and Mean Transit Time in Patients Presenting with Hyperacute Stroke. Radiology.

Stewart GN. 1894. Researches on the circulation time in organs and on the influences which affect it. Parts I-III. Journal of Physiology (London) 15:1-89.

Villringer A, Rosen BR, Belliveau JW, Ackerman JL, Lauffer RB, Buxton RB, Chao YS, Wedeen VJ, Brady TJ. 1988. Dynamic imaging with lanthanide chelates in

normal brain: contrast due to magnetic susceptibility effects. Magn.Reson.Med. 6:164-74.

Vogel J, Kuschinsky W. 1996. Decreased heterogeneity of capillary plasma flow in the rat whisker-barrel cortex during functional hyperemia. J.Cereb.Blood Flow Metab. 16:1300-6.

Weisskoff RM, Zuo CS, Boxerman JL, Rosen BR. 1994. Microscopic susceptibility variation and transverse relaxation: theory and experiment. Magn.Reson.Med. 31:601-10.

Wise RJ, Bernardi S, Frackowiak RS, Legg NJ, Jones T. 1983. Serial observations on the pathophysiology of acute stroke. The transition from ischaemia to infarction as reflected in regional oxygen extraction. Brain 106:197-222.

Wong EC, Buxton RB, Frank LR. 1997. Implementation of quantitative perfusion imaging techniques for functional brain mapping using pulsed arterial spin labeling [see comments]. NMR.Biomed. 10:237-49.

Yamakawa T, Yamaguchi S, Niimi H, Sugiyama I. 1987. White blood cell plugging and blood flow maldistribution in the capillary network of cat cerebral cortex in acute hemorrhagic hypotension: an intravital microscopic study. Circ.Shock 22:323-32.

Østergaard L, Chesler D, Weisskoff RM, Sorensen AG, Rosen BR. 1999. Modeling Cerebral Blood Flow and Flow Heterogeneity From Magnetic Resonance Residue Detection, Example 1.

Østergaard L, Johannsen P, Poulsen PH, Vestergaard-Poulsen P, Asboe H, Gee A, Hansen SB, Cold GE, Gjedde A, Gyldensted C. 1998a. Cerebral Blood Flow Measurements by MRI Bolus Tracking: Comparison with [15O]H2O PET in Humans. J.Cereb.Blood Flow Metab. 18:935-40.

Østergaard L, Smith DF, Vestergaard-Poulsen P, Hansen SB, Gee A, Gjedde A, Gyldensted C. 1998b. Absolute Cerebral Blood Flow and Blood Volume Measured by MRI Bolus Tracking: Comparison with PET Values. J.Cereb.Blood Flow Metab. 18:425-32.

Østergaard L, Sorensen AG, Kwong KK, Weisskoff RM, Gyldensted C, Rosen BR. 1996a. High resolution measurement of cerebral blood flow using intravascular tracer bolus passages. Part II: Experimental comparison and preliminary results. Magn.Reson.Med. 36:726-36

Østergaard L, Weisskoff RM, Chesler DA, Gyldensted C, Rosen BR. 1996b. High resolution measurement of cerebral blood flow using intravascular tracer bolus passages. Part I: Mathematical approach and statistical analysis. Magn.Reson.Med. 36:715-25

50

CLAIMS

1. Method for determining haemodynamic indices of an organ or of a part of tissue of a mammal including

a) determining a time series of tomographic data pertaining to the organ or part of tissue during and after a bolus injection of a tracer dose to said mammal, the tracer being substantially intravascular in said tissue,

b) determining a time series of concentration data being indicative of the concentration of the tracer in arteries of the organ or tissue from the time series of tomographic data,

c) determining a residue function of the organ or of the part of tissue by deconvolution of the time series of tomographic data with the time series of concentration data, and

d) determining a distribution of transit times from the slope of the residue function.

2. Method according to claim 1, wherein a probability density function (PDF) of a normalised haemodynamic index is determined from the distribution of transit times, the index being normalised by the value of the integral of said index.

3. Method according to claim 2, wherein at least one of the haemodynamic indices is a quantitative haemodynamic parameter obtained from the PDF.

4. Method according to claim 3, wherein at least one of the at least one parameter is obtain from comparison of the determined PDF and a previously determined reference PDF.

5. Method according to claim 4, wherein the parameter is obtained by use of the Kolmogorov Smirnov test.

6. Method according to claim 3 and comprising the steps of

determining the impulse response function of the organ or of the part of tissue by deconvolution of the time series of tomographic data with the time series of concentration data,

determining the relative tissue flow from the impulse response function of the organ or of the part of tissue,

normalising said time series of concentration data with the integral of said time series of concentration data with respect to time,

determining the normalised relative tissue flow, respectively the normalised blood volume, of the organ or part of tissue by use of the relative tissue flow and the time series of normalised concentration data, and

converting said normalised relative tissue flow, respectively normalised blood volume, to an absolute value for the tissue flow, respectively the blood volume, by means of a previously determined conversion factor,

the quantitative haemodynamic parameter being of metabolic significance and determined from the PDF and the absolute tissue flow (F_t), respectively the absolute blood volume.

7. Method according to claim 3 and claim 6, wherein a parameter (E) significant for the local extraction of a substance is determined, the method further comprising the following steps:

calculating the relative flow heterogeneity (w(f)) as a function of the relative flow (f) from the distribution of transit times,

estimating a value (P) for the local capillary permeability,

estimating a value (S) for the local capillary surface area,

calculating said parameter (E) as the integral value of the relative flow heterogeneity (w(f)) multiplied by one minus the natural exponential function of the negative ratio between

i) the product of the local capillary permeability (P) and the local capillary surface area (S), and

ii) the product of the relative flow (f) and the absolute tissue flow (F_t)

with respect to the relative flow (f).

8. Method according to claim 6 or 7, wherein the normalised relative tissue flow, respectively the blood volume, is also normalised with the ratio between body weight of the individual mammal and the injected tracer dose.

9. Method according to any of claims 6-8, wherein the previously determined conversion factor is in general applicable for the present method to members of a mammalian specie.

10. Method according to any of claims 6-9, wherein the previously determined conversion factor is in general applicable for the present method to an organ or tissue of the mammalian specie.

11. Method according to any of claims 6-10, wherein the previously determined conversion factor is a constant factor applicable for the present method for any organ or any part of tissue of the mammalian specie.

12. Method according to any of claims 6-11, wherein the previously determined conversion factor is a constant factor applicable for all of cerebral tissue of the mammalian specie.

13. Method according to any of the preceding claims, wherein the tomographic data are obtained by means of magnetic resonance imaging.

14. Method according to any of the preceding claims, wherein the tissue is cerebral tissue.

15. Method according to claim 14, wherein the tomographic data are obtained by means of susceptibility contrast magnetic resonance imaging.

16. Method according to any of the preceding claims, wherein the tomographic data comprise information pertaining to subregions of sections of the organ or part of tissue and the haemodynamic indices are determined for at least a substantial part of said subregions.

17. Method according to claim 3 and 16, wherein quantitative haemodynamic parameters are represented as images subdivided into a plurality of pixels each representing a quantitative haemodynamic parameter pertaining to one of said subregions.

18. A system for processing of time series of tomographic data pertaining to an organ or a part of tissue according to any of claims 1-17, said system residing on a computer having means for producing an output representative of at least some of the determined haemodynamic indices.

19. Method for evaluating the efficacy of a drug or a substance on an organ or on a part of tissue of a mammal by means of haemodynamic indices of said organ or of said part of tissue obtained by a method according to any of claims 1-17.

20. Method according to claim 19, wherein a system according to claim 18 is used.

21. Method for obtaining information of the likelihood of recovery of an organ or part of tissue in a living mammal upon or during a period of insufficient vascular supply of said organ or of said part of tissue in the mammal comprising determining haemodynamic indices according to claims 1-17.

22. Method for obtaining information relevant for discrimination between relevant therapy of an organ or part of tissue in a living mammal upon or a period of insufficient vascular supply of said organ or of said part of tissue in the mammal comprising determining haemodynamic indices according to claims 1-17.

23. Use of information obtained by use of the method according to any of claims 1-17 or any of claims 19-22 for preparing a reference table for use in discrimination of a

treatment schedule for an individual mammal or group of mammals for which information have been obtained in a manner similar to said information.

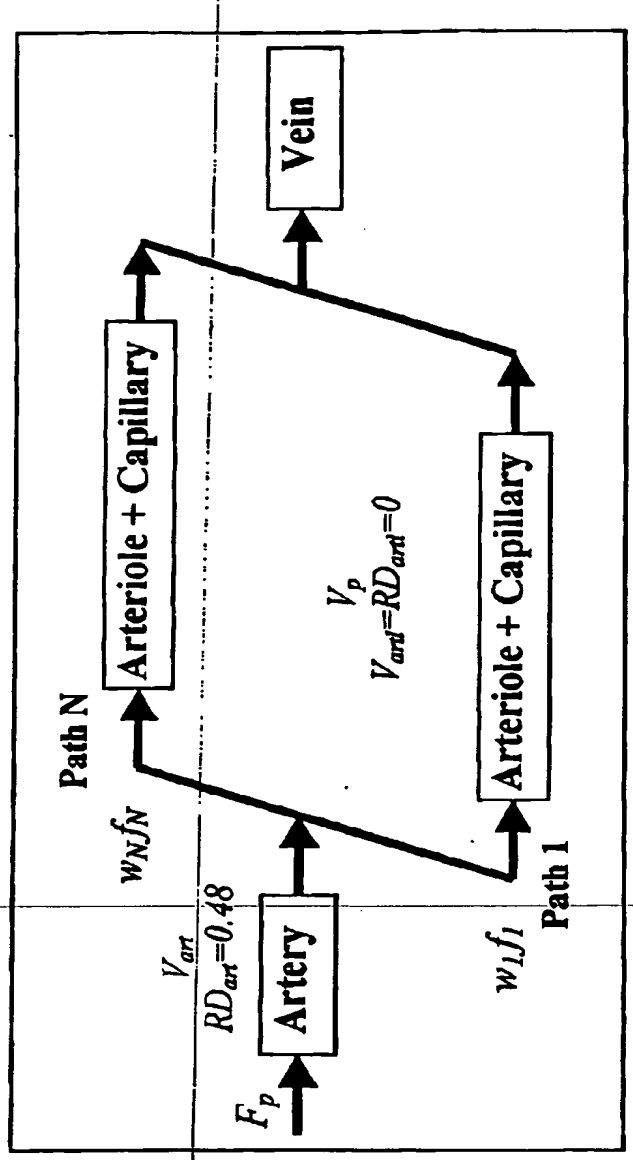
Vein
Arteriole + Capillary
Arteriole + Capillary
Path N
Path 1
V_p
$V_{art}=RD_{art}=0$
$w_N f_N$
$w_1 f_1$
V_{art}
$RD_{art}=0.48$
Artery
F_p

Fig. 1

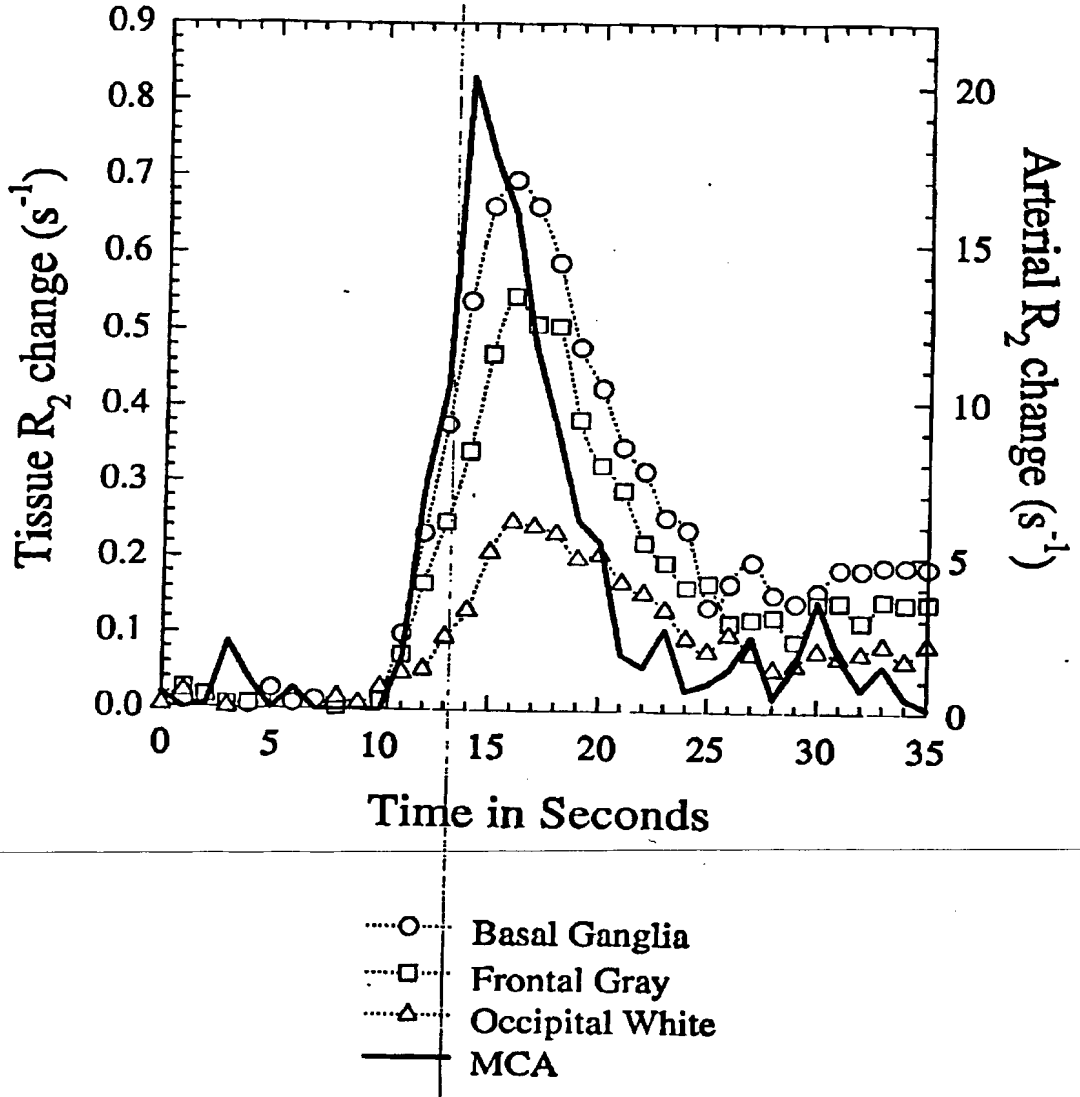
Tissue R_2 change (s^{-1})
Arterial R_2 change (s^{-1})
Time in Seconds
0.0
0.1
0.2
0.3
0.4
0.5
0.6
0.7
0.8
0.9
0
5
10
15
20
25
30
35
Basal Ganglia
Frontal Gray
Occipital White
MCA

Fig. 2

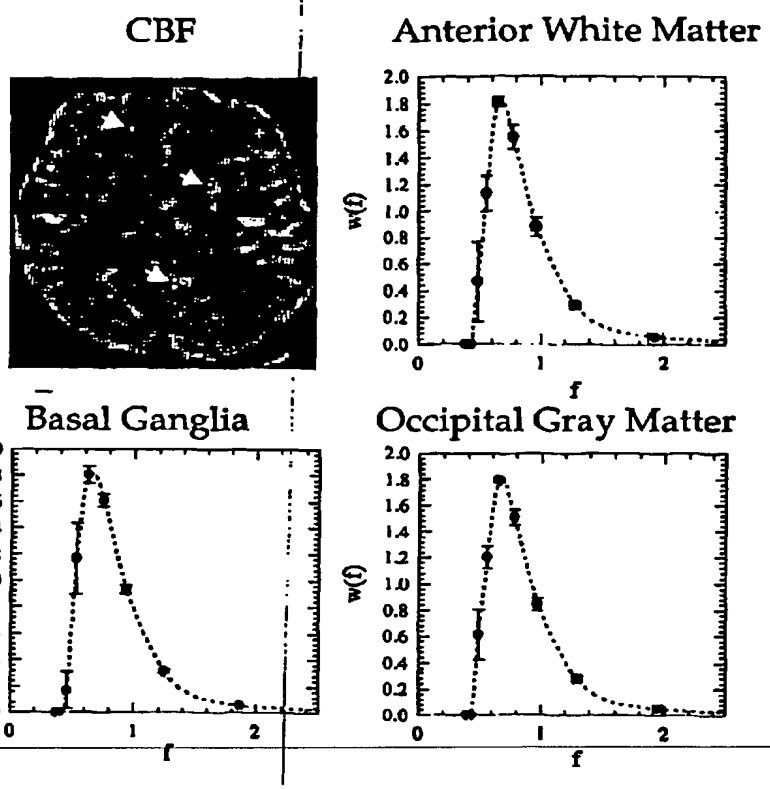
CBF
Anterior White Matter
Basal Ganglia
Occipital Gray Matter
w(f)
f
0.0
0.2
0.4
0.6
0.8
1.0
1.2
1.4
1.6
1.8
2.0
0
1
2

Fig. 3

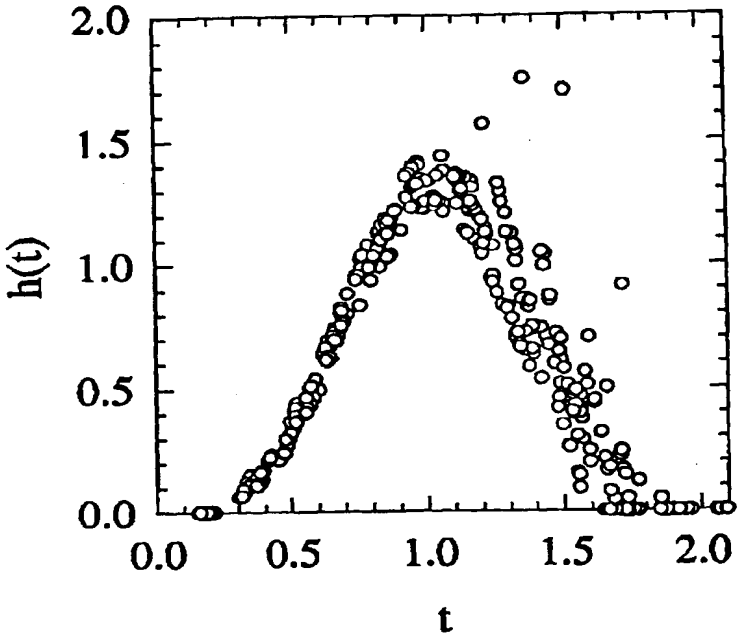

Fig. 4

Fig. 4a

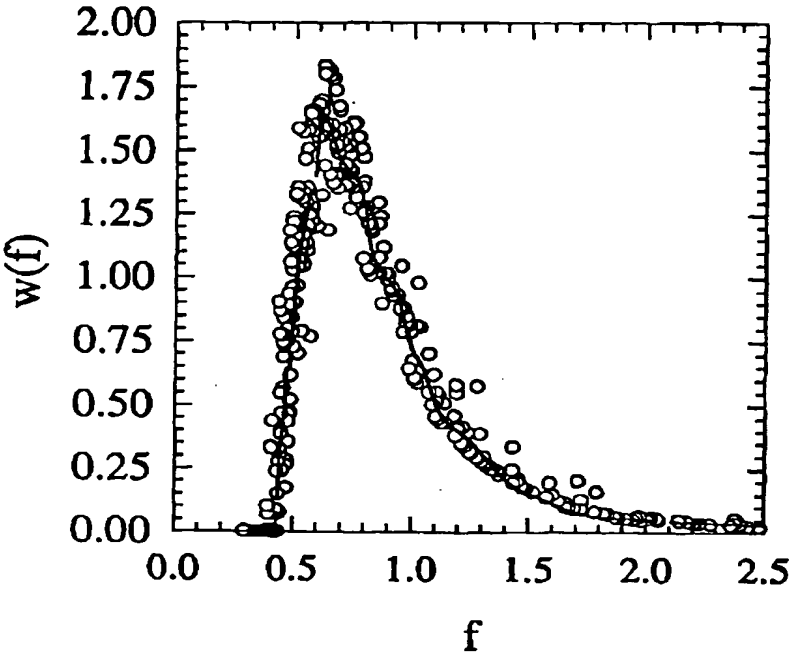

Fig. 4b

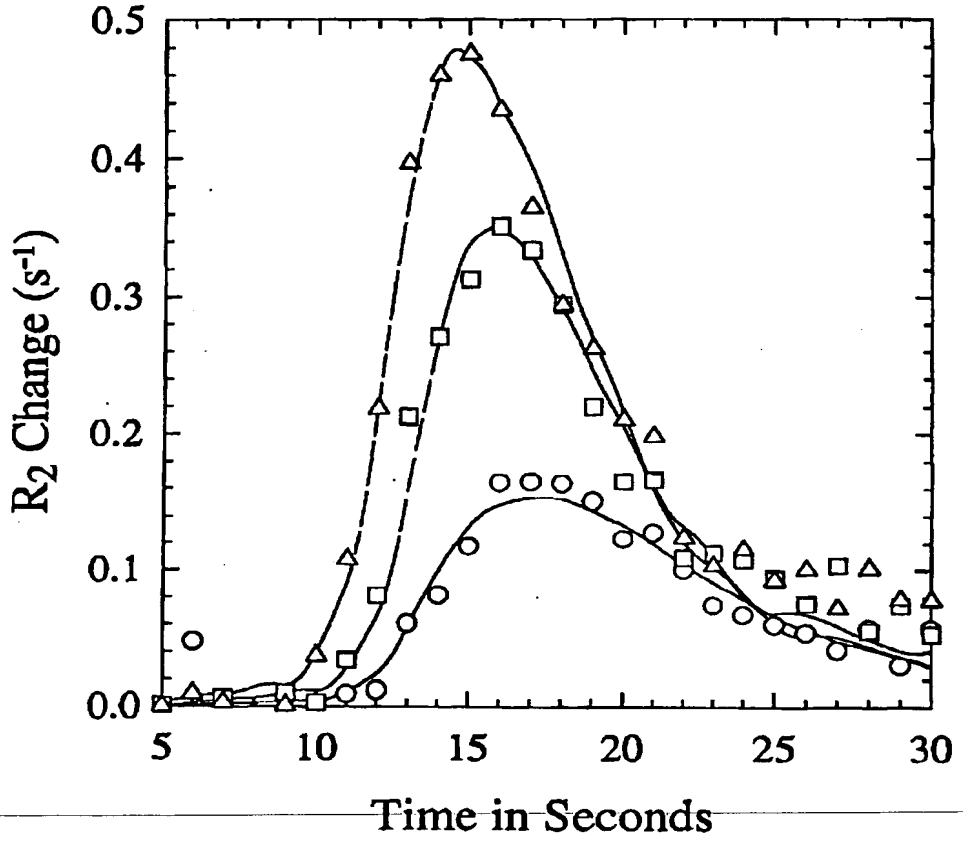
0.5
0.4
0.3
0.2
0.1
0.0
R_2 Change (s^{-1})
5
10
15
20
25
30
Time in Seconds
Occ. Gray Matter
Basal Ganglia
White Matter

Fig. 5

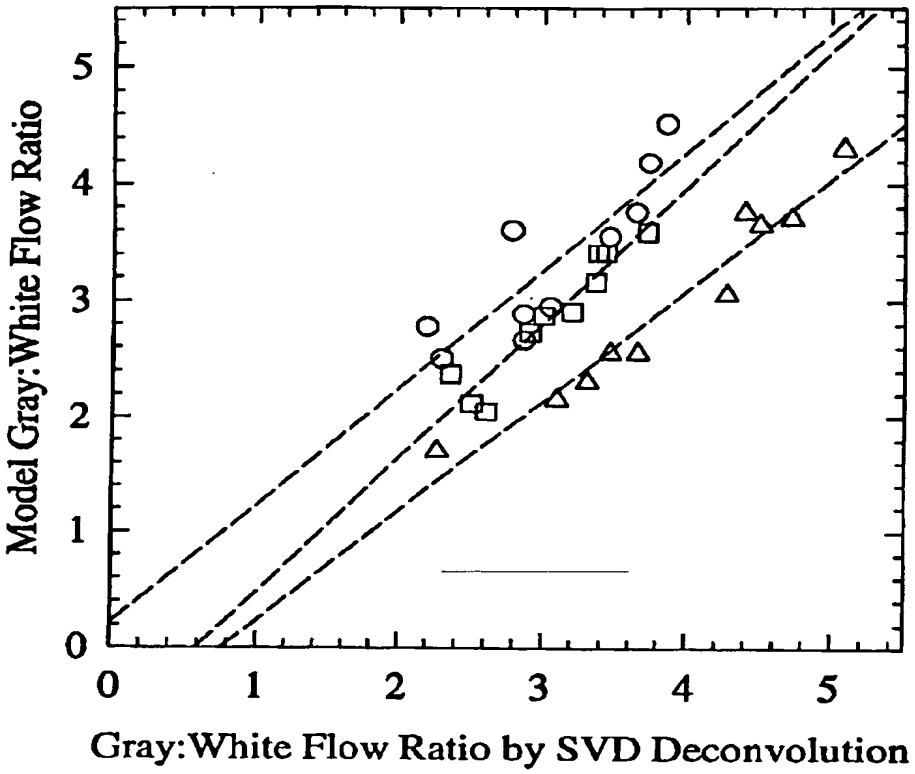
Model Gray:White Flow Ratio
0
1
2
3
4
5
Gray:White Flow Ratio by SVD Deconvolution
Volunteer 1
Volunteer 2
Volunteer 5

Fig. 6

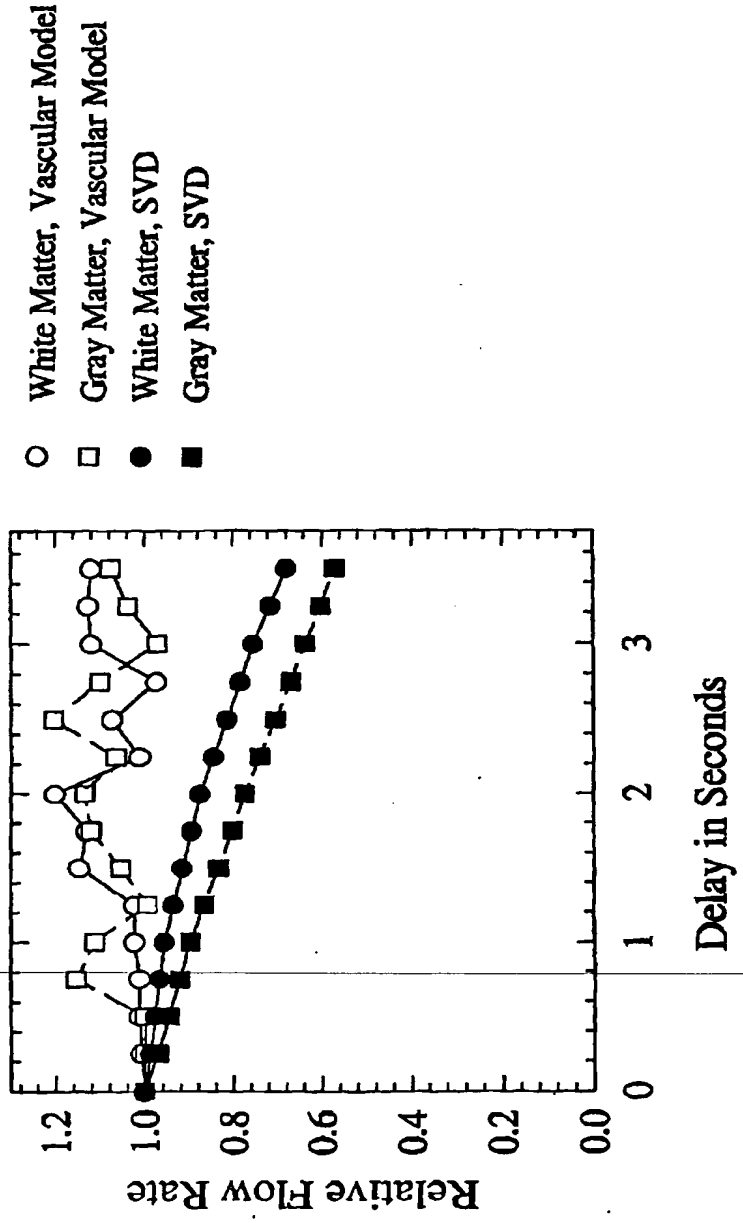
White Matter, Vascular Model
Gray Matter, Vascular Model
White Matter, SVD
Gray Matter, SVD
Relative Flow Rate
1.2
1.0
0.8
0.6
0.4
0.2
0.0
0
1
2
3
Delay in Seconds

Fig. 7a

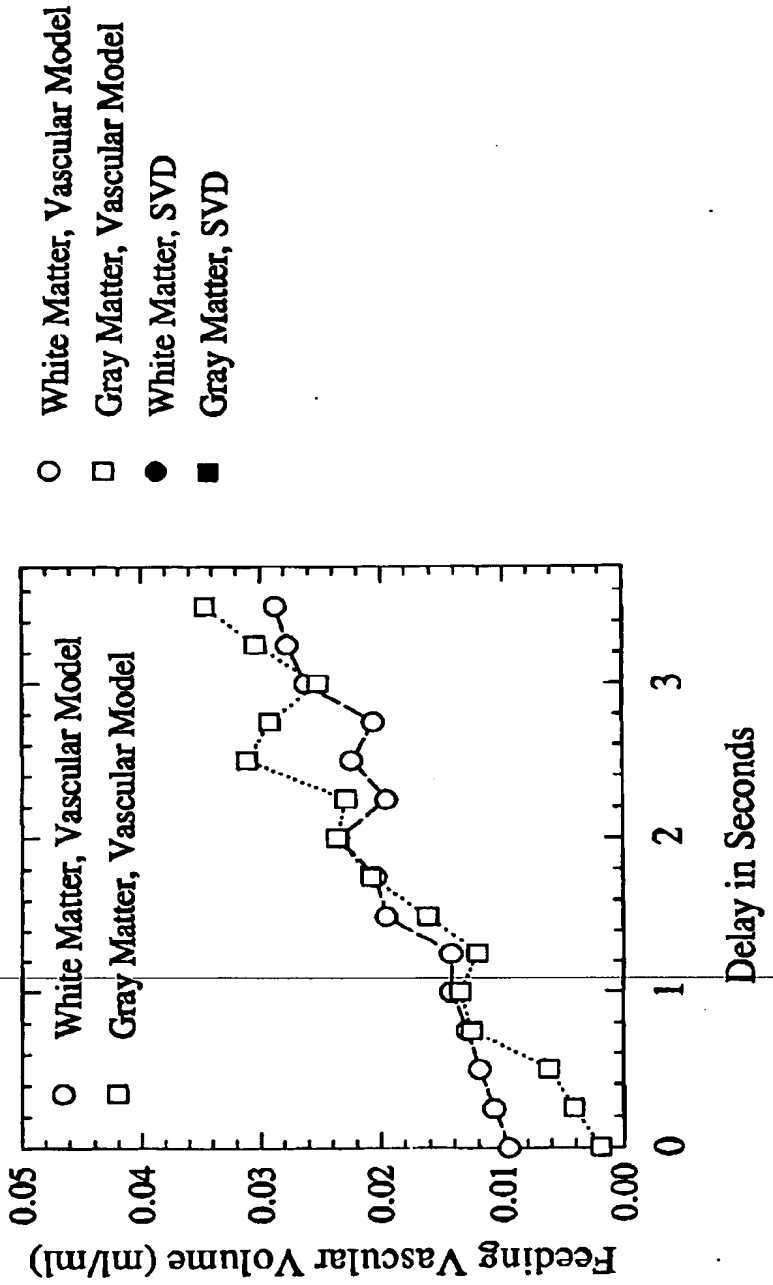
White Matter, Vascular Model
Gray Matter, Vascular Model
White Matter, SVD
Gray Matter, SVD
Feeding Vascular Volume (ml/ml)
0.05
0.04
0.03
0.02
0.01
0.00
0
1
2
3
Delay in Seconds

Fig. 7b

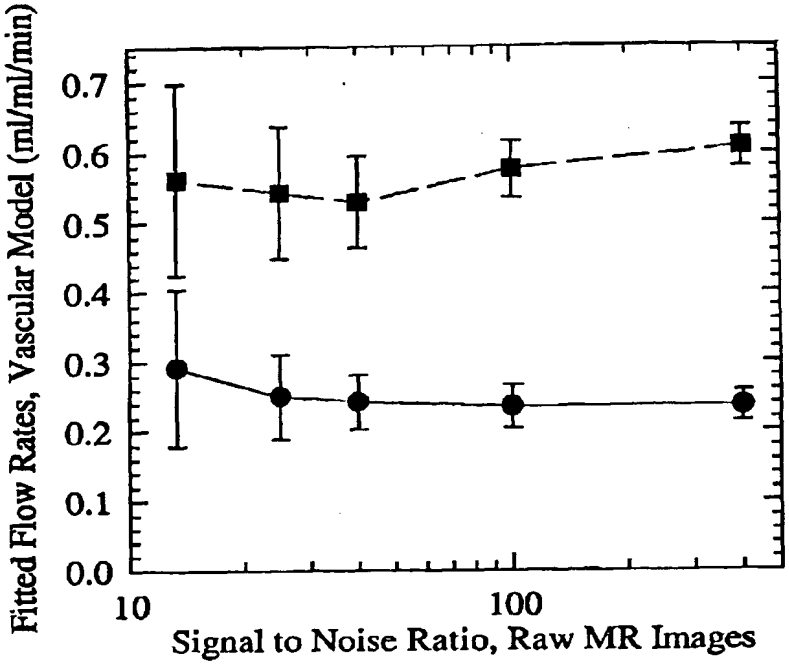
Fitted Flow Rates, Vascular Model (ml/ml/min)
0.7
0.6
0.5
0.4
0.3
0.2
0.1
0.0
10
100
Signal to Noise Ratio, Raw MR Images

Fig. 8a

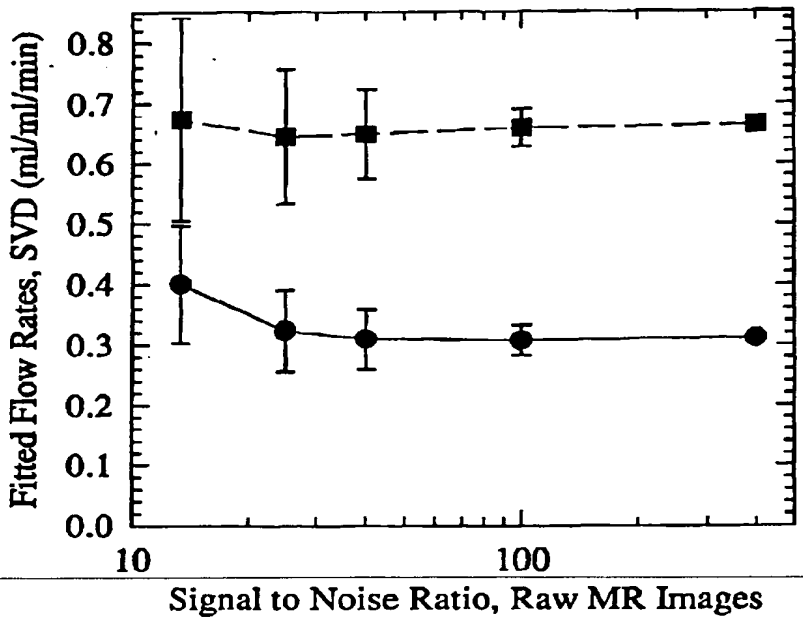
Fitted Flow Rates, SVD (ml/ml/min)
0.8
0.7
0.6
0.5
0.4
0.3
0.2
0.1
0.0
10
100
Signal to Noise Ratio, Raw MR Images

Fig. 8b

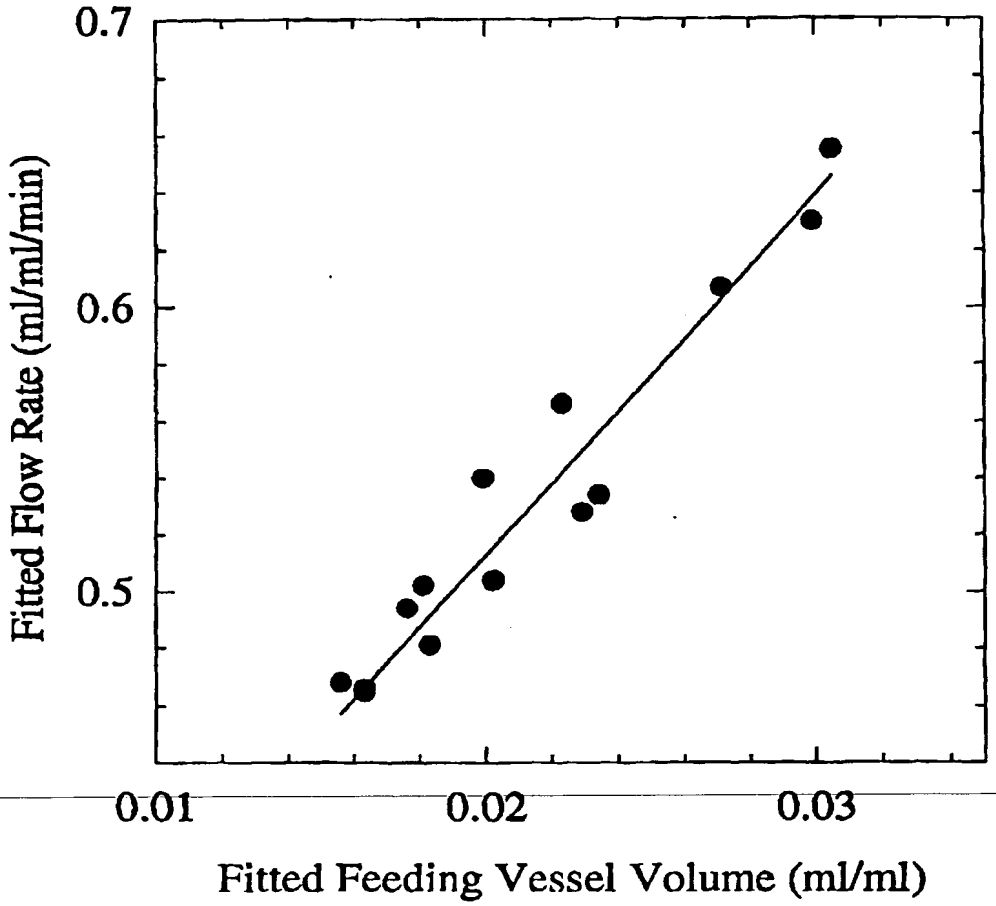
0.7
0.6
0.5
Fitted Flow Rate (ml/ml/min)
0.01
0.02
0.03
Fitted Feeding Vessel Volume (ml/ml)

Fig. 9

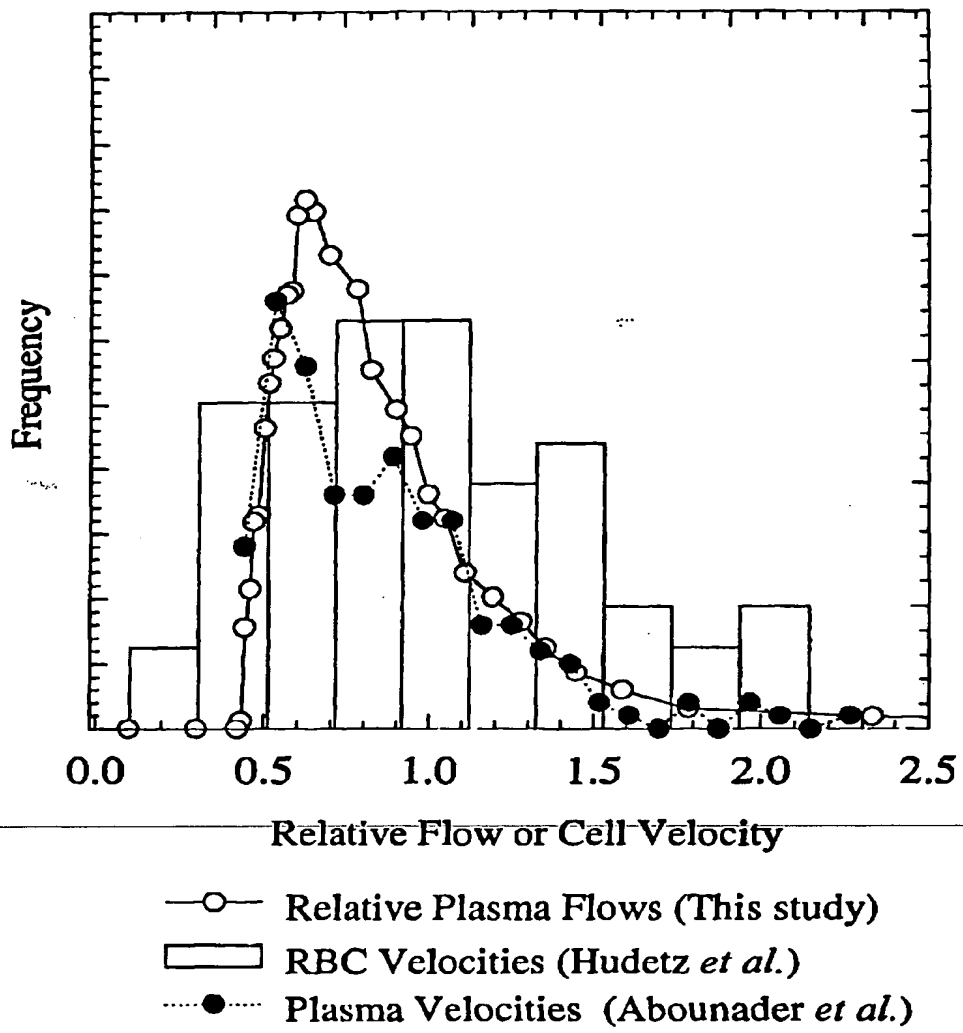
Frequency
0.0
0.5
1.0
1.5
2.0
2.5
Relative Flow or Cell Velocity
Relative Plasma Flows (This study)
RBC Velocities (Hudetz *et al.*)
Plasma Velocities (Abounader *et al.*)

Fig. 10

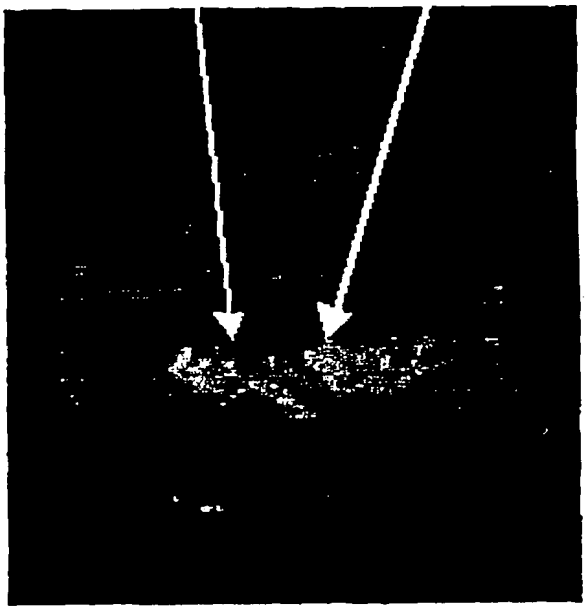

Fig. 11a

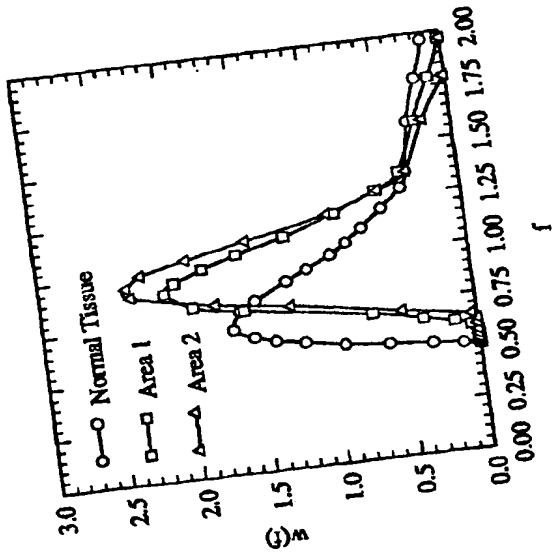
Normal Tissue
Area 1
Area 2
3.0
2.5
2.0
1.5
1.0
0.5
0.0
0.00 0.25 0.50 0.75 1.00 1.25 1.50 1.75 2.00
f

Fig. 11b

p

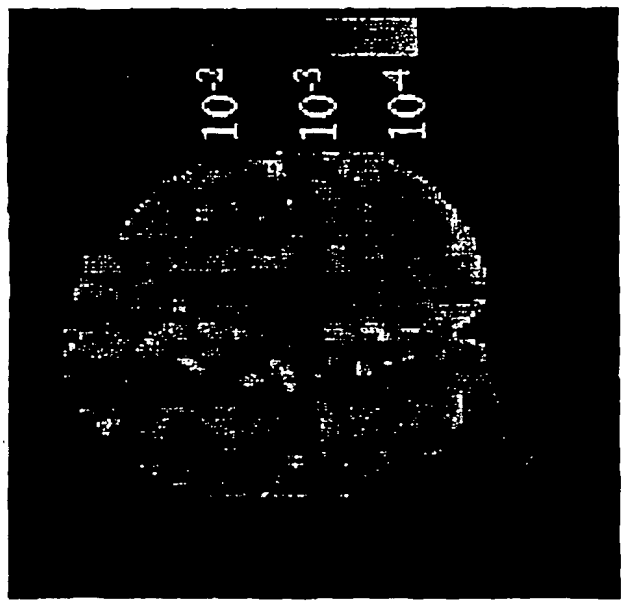

Acute p on CBF map

Fig. 11c

17/25

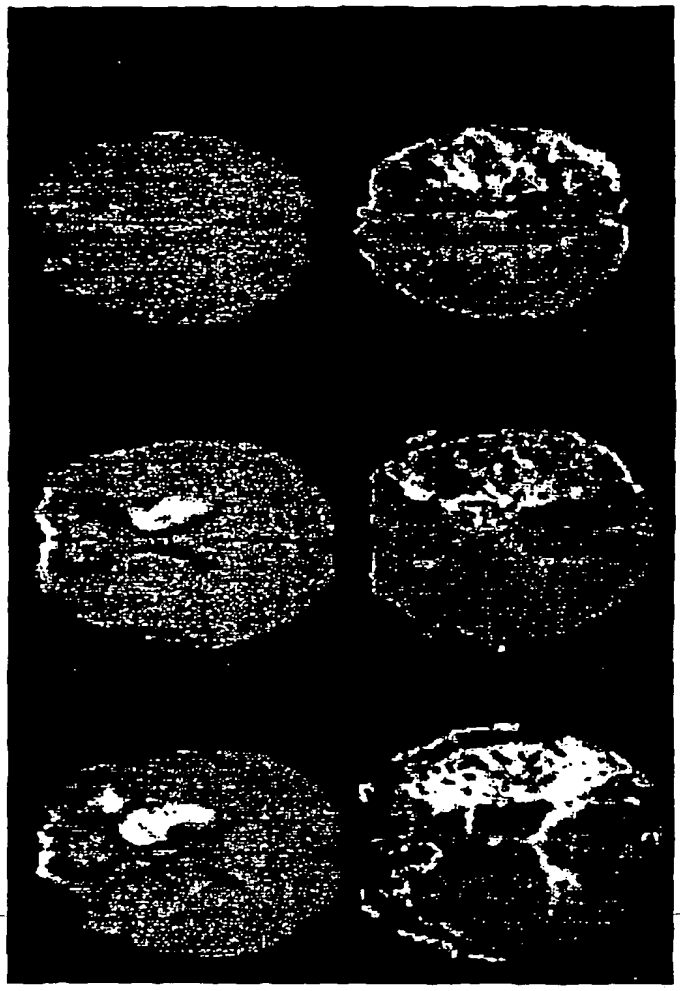

Fig. 12a

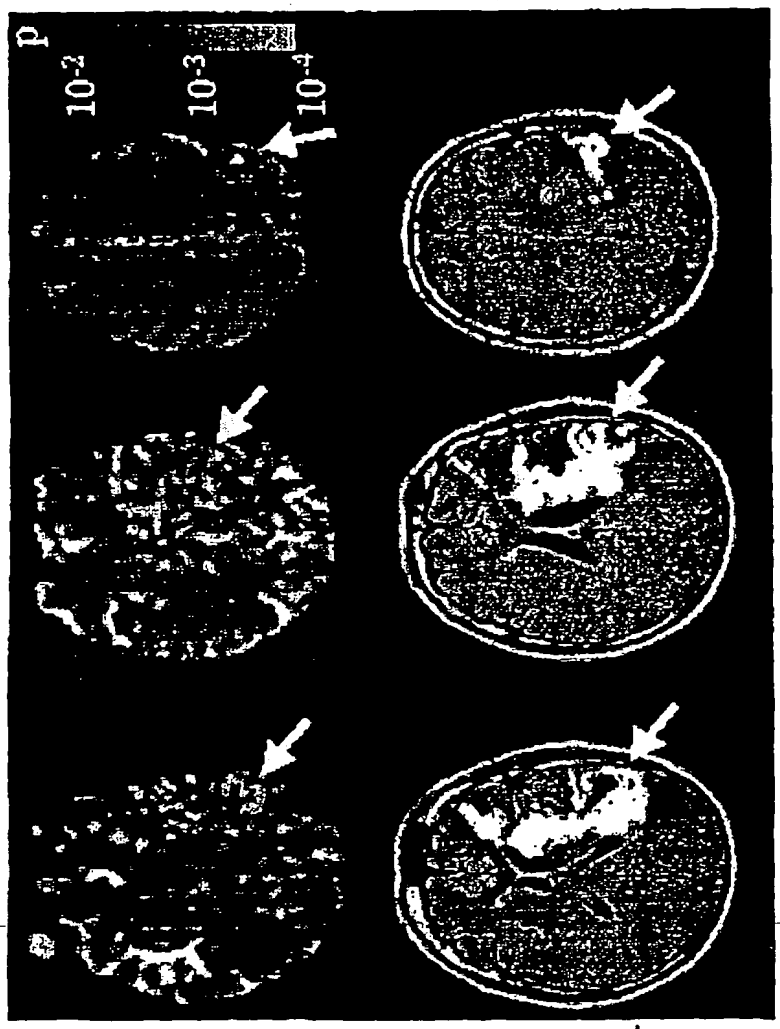

Fig. 12b

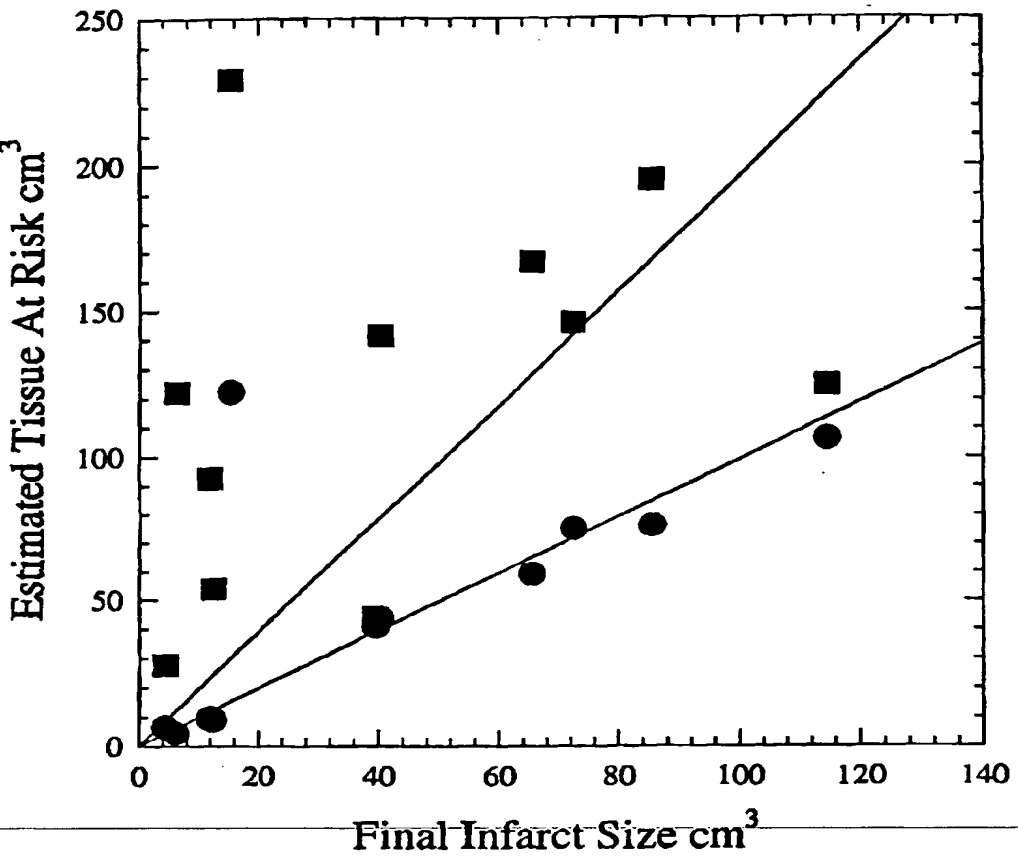
250
200
150
100
50
0
0
20
40
60
80
100
120
140
Estimated Tissue At Risk cm3
Final Infarct Size cm3
Initial DWI + Heterogeneity
Initial DWI + MTT

Fig. 13

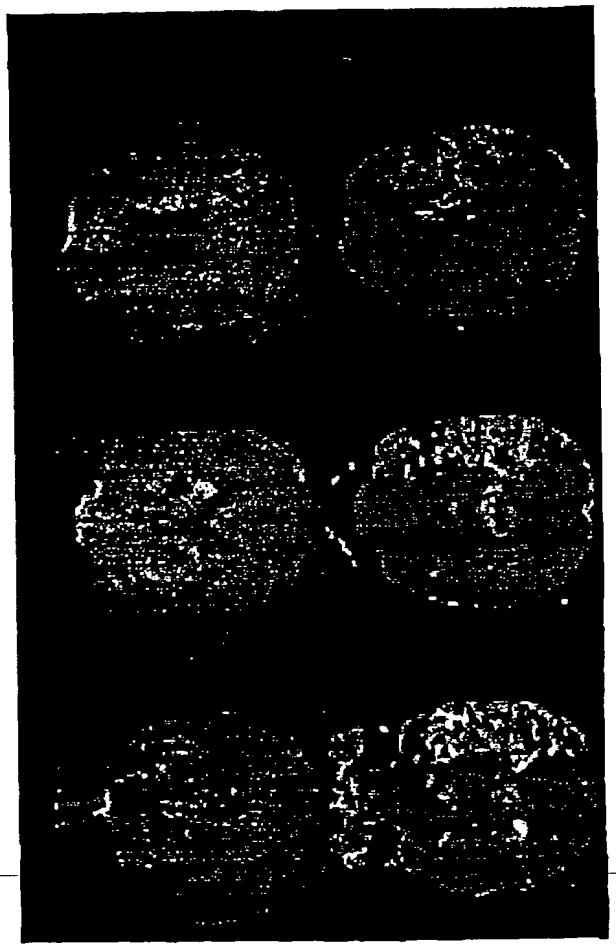

Fig. 14a

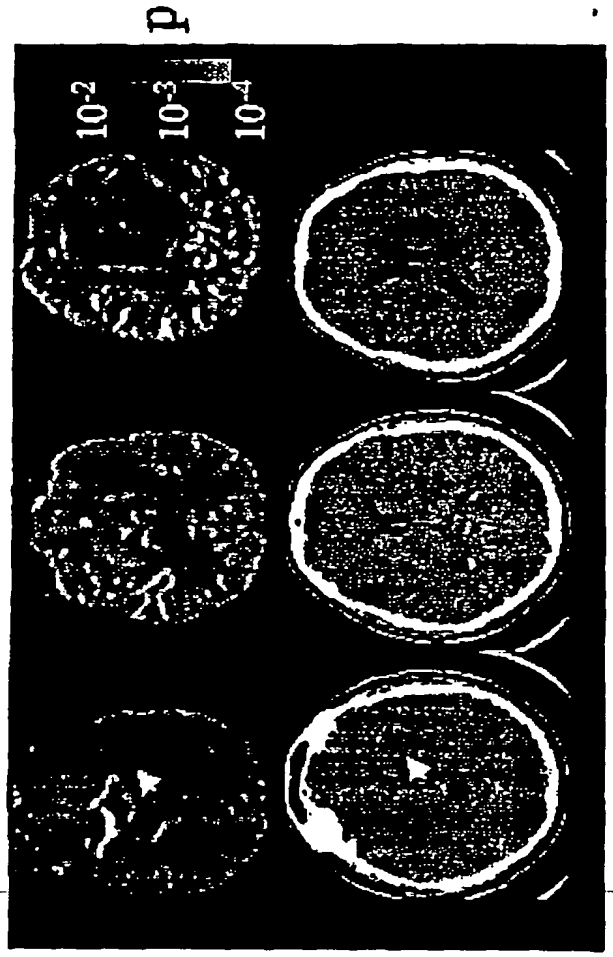

Fig. 14b

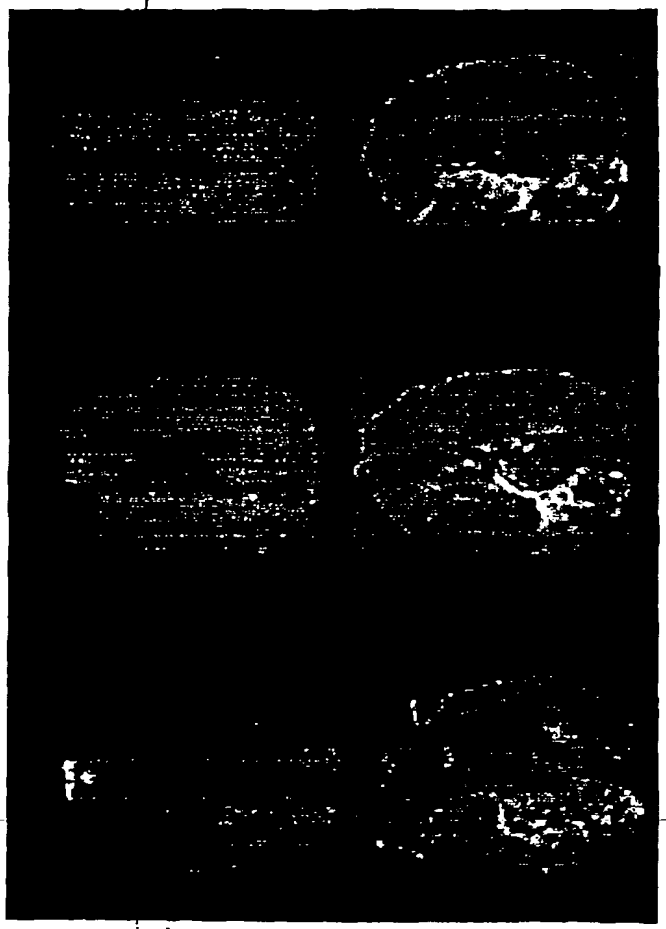

Fig. 15a

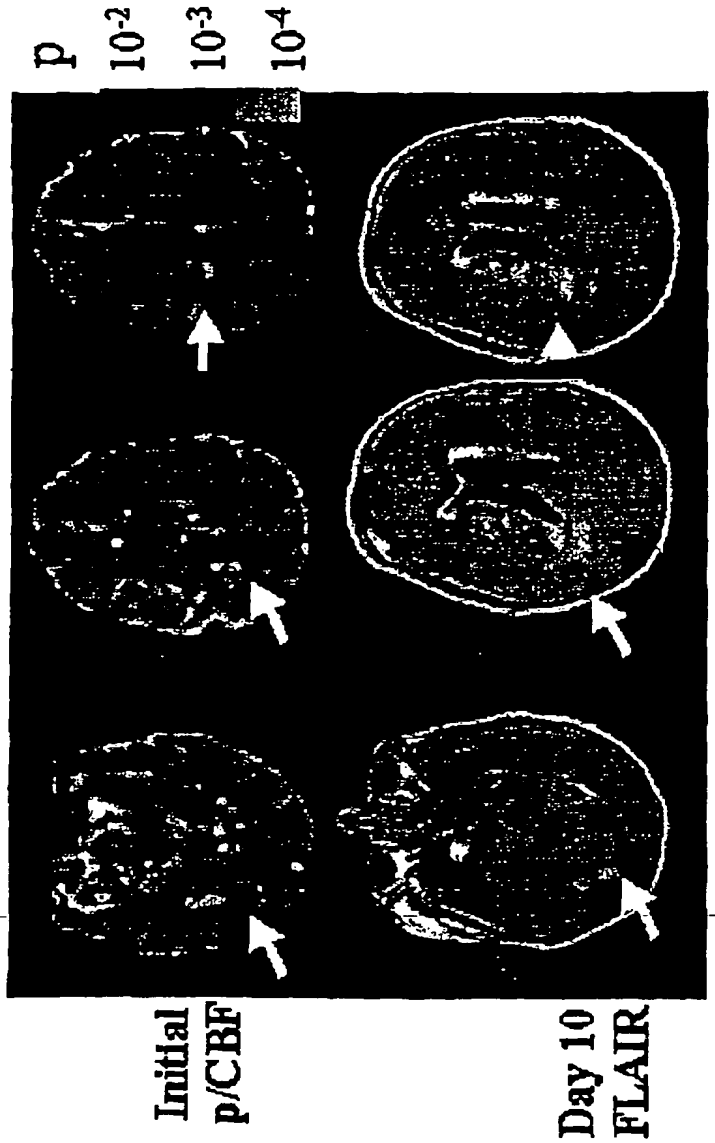

Fig. 15b

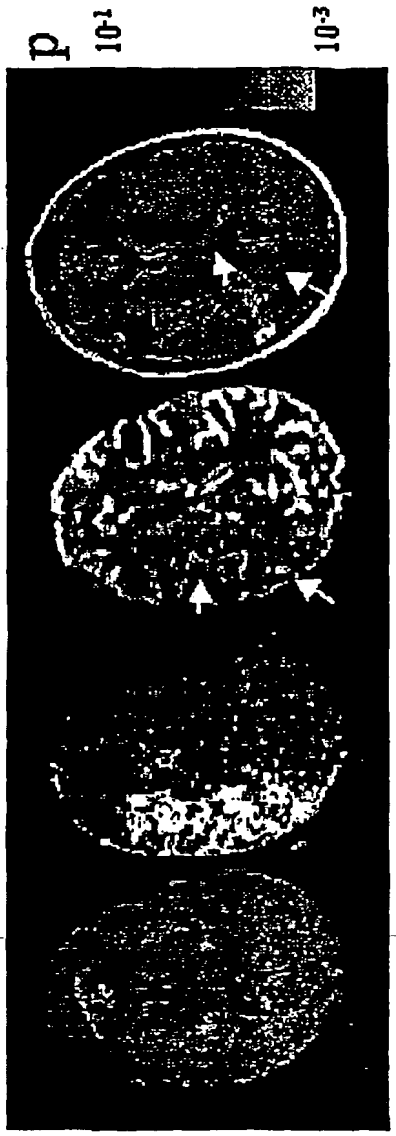

Fig. 16

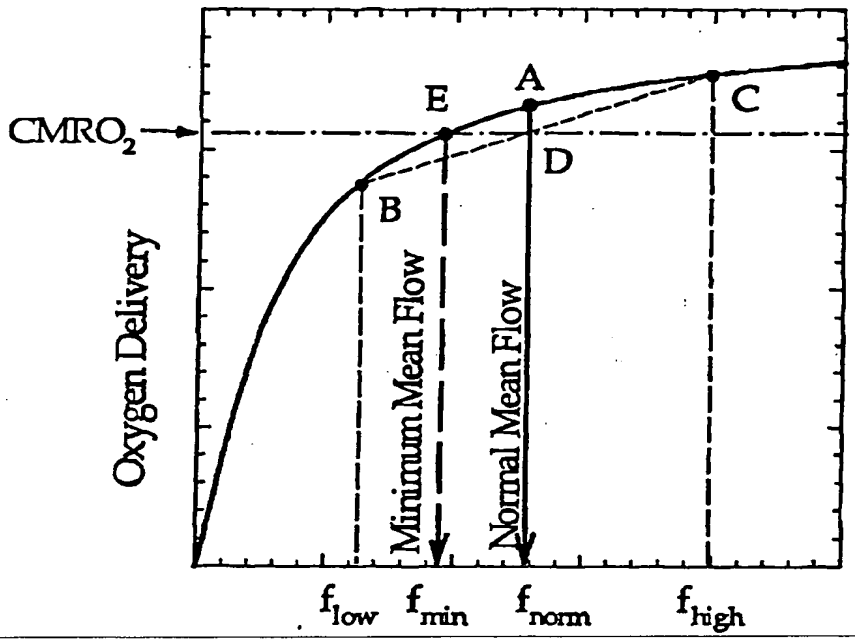
CMRO2
E
A
C
D
B
Oxygen Delivery
Minimum Mean Flow
Normal Mean Flow
flow
fmin
fnorm
fhigh
Flow

Fig. 17

THIS PAGE BLANK (USPTO)